DEVELOPMENT OF A MODEL FOR THE PREDICTION OF THE EFFECTS OF

MULTIPLE DISTINCT MODES OF NONLINEARITY ON RAIL BUCKLING

A Dissertation

by

VALENTINA MUSU

Submitted to the Graduate and Professional School of
Texas A&M University
in partial fulfillment of the requirements for the degree of

DOCTOR OF PHILOSOPHY

Chair of Committee,	David H. Allen
Committee Members,	Juan J. Horrillo
	Theofanis Strouboulis
	Yong-Rak Kim
Head of Department,	Sharath Girimaji

August 2023

Major Subject: Ocean Engineering

ABSTRACT

A model is developed herein for predicting the onset of environmentally induced buckling in rail structures. As described below, the model may be considered to be an extension of previous efforts spanning much of the twentieth century, and particularly should be considered as an extension of the three degree of freedom model presented in the CRR Report No. 2017-01 (Allen and Fry, 2017) as well as the efforts presented in the derivative M. S. Thesis (Musu 2021). Building on both previous analytic and computational solutions, a finite element model is developed for the purpose of predicting buckling as a function of the track and support structure material properties, the track and support system geometries, the applied track loading, and the initial lateral displacement within the track. Particular emphasis is placed on nonlinearity and history dependence of the track environment. The model is capable of handling multiple distinct modes of nonlinearity: geometric nonlinearity due to large deformations and track misalignment, constitutive nonlinearity due to nonlinear friction at the ballast-tie interface and due to track uplift. The resulting algorithm is deployed herein to solve problems demonstrating usefulness of the model.

DEDICATION

[…]
“[V]incer potero dentro a me l’ardore
ch’i’ ebbi a divenir del mondo esperto
e de li vizi umani e del valore;
ma misi me per l’alto mare aperto
sol con un legno e con quella compagna
picciola da la qual non fui diserto.
L’un lito e l’altro vidi infin la Spagna,
fin nel Morrocco, e l’isola d’i Sardi,
e l’altre che quel mare intorno bagna.
[…]
"O frati," dissi, "che per cento milia
perigli siete giunti a l’occidente,
a questa tanto picciola vigilia
d’i nostri sensi ch’è del rimanente
non vogliate negar l’esperïenza,
di retro al sol, del mondo sanza gente.
Considerate la vostra semenza:
fatti non foste a viver come bruti,
ma per seguir virtute e canoscenza".”

Dante Alighieri, La Divina Comedia, L’Inferno, XXVI, 97-120

ACKNOWLEDGEMENTS

I would like to thank my committee chair, Dr. Allen, for his invaluable advice, support, and immeasurable patience as well as mentorship throughout my graduate studies. I truly appreciate having had the life changing opportunity to further my education and to learn from you, both as a student and as a person.

I would also like to thank my committee members, Dr. Horrillo, Dr. Strouboulis and Dr. Kim for their guidance and encouragement throughout the course of this research. Thanks also go to my friends and colleagues in the Department of Ocean Engineering, and to the faculty and staff that have helped shape my experience at Texas A&M.

Finally, I would like to warmly thank all my friends and family that have stood by me and the choices I have made for my life. To Alexandra for helping me live out my childhood dreams and helping me rediscover the joy and excitement of pursuing something new and pushing me to give it my all. To my dear friends at the Texas A&M Figure Skating Club for keeping me grounded and believing in me even when I did not believe in myself. To Nick, Alan, Vicki, Joe, Tobia, Aldo, Caria, Patrizio e Alice for being a steading presence in my life, to Ting-Ming and Tiwi for listening to my shenanigans, to Deanna for her unconditional support, as well as every other friend I have made along the way: you know who you are, you are loved, and you are appreciated.

A Mamma, per avermi lasciato piangere quando ne avevo voglia, e a Papà per avermi spronato a non mollare. Grazie, grazie, grazie.

CONTRIBUTORS AND FUNDING SOURCES

Contributors

This work was supervised by a dissertation committee consisting of Dr. Allen and Dr. Horrillo from the Department of Ocean Engineering, Dr. Strouboulis from the Department of Aerospace Engineering and Dr. Kim from the Department of Civil and Environmental Engineering.

This work should be considered an extension of the model presented in CRR Report No. 2017-01 by D. H. Allen and G. Fry published in 2017, as well as an extension of the M.S. Thesis I completed in 2021. Therefore, the work presented in Chapters I-IV was partially reproduced with the permission of the authors.

All other work conducted for the thesis was completed by the student independently.

Funding Sources

Graduate study was supported by the means of a graduate research assistantship funded by Dr. Allen and MxV Rail. The authors are grateful to the Association of American Railroads for the support provided for this research under contract.

NOMENCLATURE

A	Twice the cross-sectional area of the rail
AAR	The Association of American Railroads
DOF	Degree of Freedom
E	Young's modulus of the rail
e	Generic finite element
FEM	Finite Element Method
FRA	The Federal Railroad Administration
I_{yy}	Twice the moment of inertia of the rail about the y axis
I_{zz}	Twice the moment of inertia of the rail about the z axis
k_x	The x-component of the coefficient of friction of the rail-ballast system
k_y	The y-component of the coefficient of friction of the rail-ballast system
k_y^0	The initial y-component of the nonlinear coefficient of friction
k_y^1	The final y-component of the nonlinear coefficient of friction
k_z	The track modulus of the rail ballast system
L	The length of the buckled region of the rail
L_e	The length of a generic element of the discretized domain
M_y	The resultant moment about the y coordinate axis
M_z	The resultant moment about the z coordinate axis
n	The exponent for the nonlinear friction power law fitting parameter
$P^T = EA\alpha\Delta T$	The thermally induced axial force resultant in the x coordinate direction

p_x	The externally applied force per unit length in the x coordinate direction
p_y	The externally applied force per unit length in the y coordinate direction
p_z	The externally applied force per unit length in the z coordinate direction
RNT	The Rail Neutral Temperature
$u(x)$	The displacement of the centroid of the rail in the x coordinate direction
u_i	The displacement vector in tensorial notation
u_i^e	The axial displacement component at the i^{th} end of element e
v_0	The denominator for the nonlinear friction power law fitting parameter
$v(x)$	The displacement of the centroid of the rail in the y coordinate direction
v_i^e	The lateral displacement component at the i^{th} end of element e
V_y	The lateral force resultant in the y coordinate direction
V_z	The vertical force resultant in the z coordinate direction
$w(x)$	The displacement of the centroid of the rail in the z coordinate direction
w_i^e	The vertical displacement component at the i^{th} end of element e
x	The coordinate axis in the longitudinal direction of the rail structure
x_i	The spatial coordinate reference vector in tensorial notation
X_i	The material coordinate reference vector in tensorial notation
y	The coordinate axis in the horizontal direction of the rail structure
$\bar{y}$	The horizontal distance from the centroid
z	The coordinate axis in the vertical direction of the rail structure
$\bar{z}$	The vertical distance from the centroid
α	The coefficient of thermal expansion of the rail

ΔT	The temperature change of the rail from the rail neutral temperature
ε_{xx}	The axial strain within the rail
θ_y	The rotation of the rail neutral surface about the y coordinate axis
θ_{yi}^e	The rotation component about the y axis at the i^{th} end of element e
θ_z	The rotation of the rail neutral surface about the z coordinate axis
θ_{zi}^e	The rotation component about the z axis at the i^{th} end of element e
σ_{xx}	The normal component of stress in the x direction

TABLE OF CONTENTS

LIST OF FIGURES

Page

LIST OF TABLES

Page

CHAPTER I

INTRODUCTION*

Rails are known to undergo a variety of failure mechanisms that can cause significant property damage and loss of life (FRA 2020). It is therefore propitious to develop advanced models for the purpose of mitigating such mishaps. Toward this end, one such model is presented herein.

A common cause of rail misalignment is so-called thermal buckling, as shown in Fig. 1. The Federal Railroad Administration (FRA 2020) reports that there have been 6,862 rail accidents within the United States in the last four years. Of these, approximately 0.7% are listed as being caused by rail buckling. However, an additional 10% of reported accidents may be related to thermal buckling such as broken rail bases (1.0%), buff/slack action excess (1.9%), kicking or dropping cars (2.2%), head shelling (2.3%), harmonic rock off (1.6%), and transverse/compound fissure (1.0%). These reported figures suggest that thermal buckling may be a causal factor in significant loss of life and damage costing perhaps as much as billions of dollars.

Unfortunately, guidelines for mitigating the effects of buckling in rails have not to date been developed, and this is due at least in part to the fact that buckling is a rather complicated phenomenon caused by the following factors: temperature distribution within the rail, rail pinning, crosstie balance, lateral track-walk, friction acting between the ties and the ballast, vertical lift-off and the structural configuration of the underlying railway base. Thus, there is a need to develop a technique for avoiding buckling in rails.

*Partially reproduced with permission from the author, "*Computational Model for Predicting Buckling in Rail Structures*" by Valentina Musu [2021], An unpublished Master's Thesis, Texas A&M University

Figure 1. Photograph Showing Thermally Induced Buckling of a Railway (Reprinted with Permission from Lankyrider, CC BY-SA 4.0, via Wikimedia Commons)

The literature on this subject is long and deep. Historically, Galileo introduced the problem of a beam in bending in 1637 (Galileo 1637). More than a century later, the first cogent model for beam bending was reported by Euler and Bernoulli (Euler 1744). In the early twentieth century this approach was used to model the structural response of rails (Timoshenko 1915, 1927). Over the most recent half century a rigorous beam formulation of the rail thermal buckling problem has emerged (Kerr 1974, 1978). This model has been previously deployed within the finite element method to predict lateral thermal buckling as a function of temperature, track residual deformation, nonlinear ballast interface resistance (Tvergaard and Needleman 1981). Nonlinear effects such as loss of contact between the rail and the wheel, rail lift-off from the tie and tie lift-off from the ballast have also been modelled (Dong, Sankar and Dukkipati 1994). Additionally, a significant effort has been made to investigate the stability of continuously welded rail (CWR) (Kish, Samavedam and Jeong 1985, Kish, Kalay, Hazell, Schoengart and Samavedam 1993, Kish, Clark and Thompson 1995, Kish and Samavedam 1997 and 2005, Kish, Samavedam and Wormley 2001, and Klaren and Loach 1965) and the effects of thermal buckling in rails (Kish and Samavedam 1982, 1990, 1991, 1999 and 2013, Kish, Sussman and Trosino 2003 and Kristoff 2001).

Furthermore, models excluding the effects of vehicle loads, also called static models, were developed for tangent and curved track with misalignments (Samavedam 1979, Kish and Samavedam 1991). Finally, further research was conducted to develop a dynamic model of track thermal buckling and stability (Samavedam, Kish and Jeong 1986 and 1987, Samavedam, Purple, Kish and Schoengart 1993, Samavedam 1995 and 1997, Samavedam, Kanaan, Pietrak, Kish and Sluz 1995, Samavedam et al. 1997 and Samavedam and Kish 2002).

More recently, a more detailed finite element formulation has been employed to include the effects of both fastener stiffness and vertical deformations on the prediction of lateral thermal buckling (Lim et al 2003). Furthermore, an analytical model has been developed for predicting the effects of tie and fastener resistance on lateral thermal buckling (Grissom and Kerr 2006). In order to obtain an analytical solution, however, Grissom and Kerr found it necessary to make simplifying assumptions that significantly impacted the accuracy of the predicted buckling load.

Although not focused on rail applications, geometrically nonlinear models have been developed for buckling and nonlinear post-buckling of Euler-Bernoulli beams supported on elastic foundations (Li and Batra 2007, Yang and Bradford 2016).

Furthermore, complex three-dimensional models of continuously welded rail (CWR) have been developed using commercially available FE codes for buckling analysis of tracks subjected to thermal loading under the following conditions: linear friction (Pucillo 2016), interspersed railway tracks (Kaewunruen et al. 2018) multi-body dynamic interaction in consideration of nonlinear friction and uplift of the track (Miri et al. 2021). Finally, in the oil and gas industry, offshore pipelines are known to experience somewhat similar buckling due to the transport of high-temperature or high-pressure hydrocarbons (Hobbs 1984, Taylor and Aik 1989, Miles and Calladine 1999 and Zhang and Kyriakides 2021).

Based on the above findings, it is evident that there exists a need to develop a model that is capable of simulating the buckling response of rails due to simultaneous geometric nonlinearity, elastic foundation, track lift-off, and nonlinear friction occurring at the ballast-rail interface. Such a model would need to be able to accurately represent the real-world physics of the rail structure while maintaining computational efficiency. Thus, the current research is focused on making use of the significant findings reported above to develop a computational open-source model that is both convenient to deploy and capable of accurately predicting lateral buckling in rails.

CHAPTER II

MODEL DEVELOPMENT*

Consider a generic rail mounted on a railway, as shown in Fig. 2. Note that the x coordinate axis is aligned in the direction of travel, and the y and z coordinate axes are aligned with the horizontal and vertical directions, respectively, thereby resulting in a right-handed coordinate system. Note that as a result of the right-handed coordinate system employed herein, a right-handed sign convention has also been adopted throughout the development of the model, such that a counterclockwise rotation in the x-y plane is considered positive, while a positive rotation in the x-z plane is by convention clockwise.

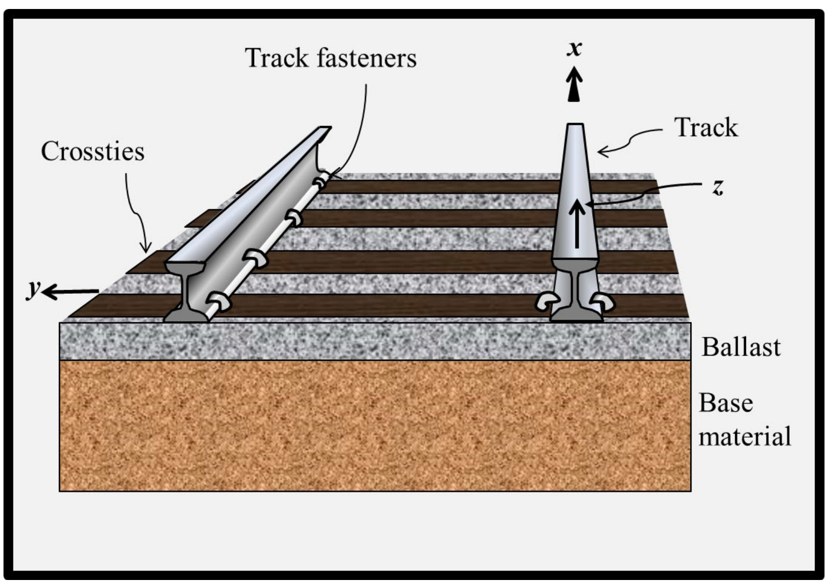

Figure 2 .Generic Rail with Right-Handed Coordinate System as Shown (Reprinted with Permission from Musu 2021)

Furthermore, as shown in Fig. 2, the track structure is composed of two rails, connected to the crossties by pins, which are in turn staked into the ballast and rest on an elastic

*Partially reproduced with permission from the author, "*Computational Model for Predicting Buckling in Rail Structures*" by Valentina Musu [2021], An unpublished Master's Thesis, Texas A&M University

foundation. Each component of the structure interacts with each other: the crossties provide the structure with additional resistance to bending, while the ballast provides stability, drainage and resistance to motion due to the ballast-tie interface friction and finally, the elastic foundation provides resistance to out-of-plane motion.

In order to construct a model for buckling of the track structure, it is assumed that the structure may be adequately modeled as a Euler-Bernoulli beam-column, implying that it is long and slender (Euler 1744, Allen and Haisler1985, Grissom and Kerr 2006). Furthermore, as Lim and coworkers (Lim et al 2003) have shown that the out-of-plane deformation component might be significant, it will be assumed herein that this component of deformation must be included in the model to accurately predict lateral buckling. Using these two assumptions and considering how the structural components of the track structure interact with each other, the track structure shown in Fig. 2 may be idealized as a single slender beam. The centroidal axis of the rail may deform in all three coordinate directions, and the components of this displacement are denoted by $u(x,t)$, $v(x,t)$ and $w(x,t)$, respectively. Similarly, the components of stress $\sigma_{xx}(x,y,z,t)$, $\sigma_{xy}(x,y,z,t)$ and $\sigma_{xz}(x,y,z,t)$ are shown on an arbitrary cross-section of the rail in Fig. 3.

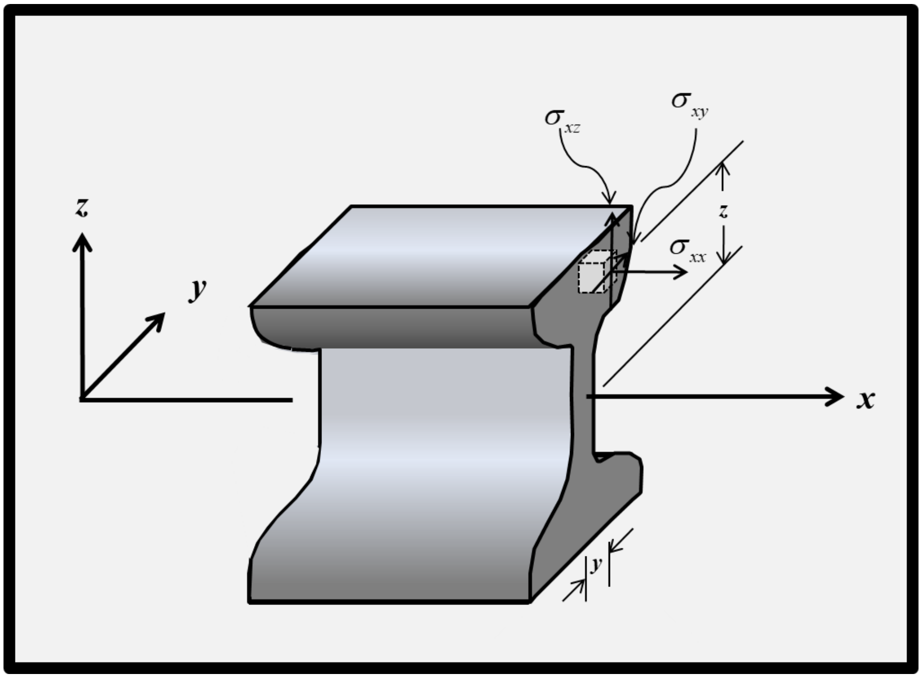

Figure 3. Components of Stress on an Arbitrary Cross-Section of the Rail (Reprinted with Permission from Musu 2021)

A top view of a free body diagram of a section of the rail is constructed in Fig. 4, wherein the load per unit length applied to the centroidal axis of the rail is composed of components $p_x(x,t)$ and $p_y(x,t)$ in the *x* and *y* coordinate directions, respectively. In addition, the normal component of force per unit length applied to the bottom of the rail due to the normal displacement component $v(x,t)$ is denoted as $-k_y v(x,t)$, where $k_y(x,t)$ is the lateral coefficient of friction and the negative sign is employed so that the base stiffness is non-negative when the resultant is positive due to lateral displacement of the rail. Similarly, the axial component of force per unit length applied to the bottom of the rail due to the axial component of displacement $u(x,t)$ is denoted as $-k_x u(x,t)$, where $k_x(x,t)$ is the axial coefficient of friction.

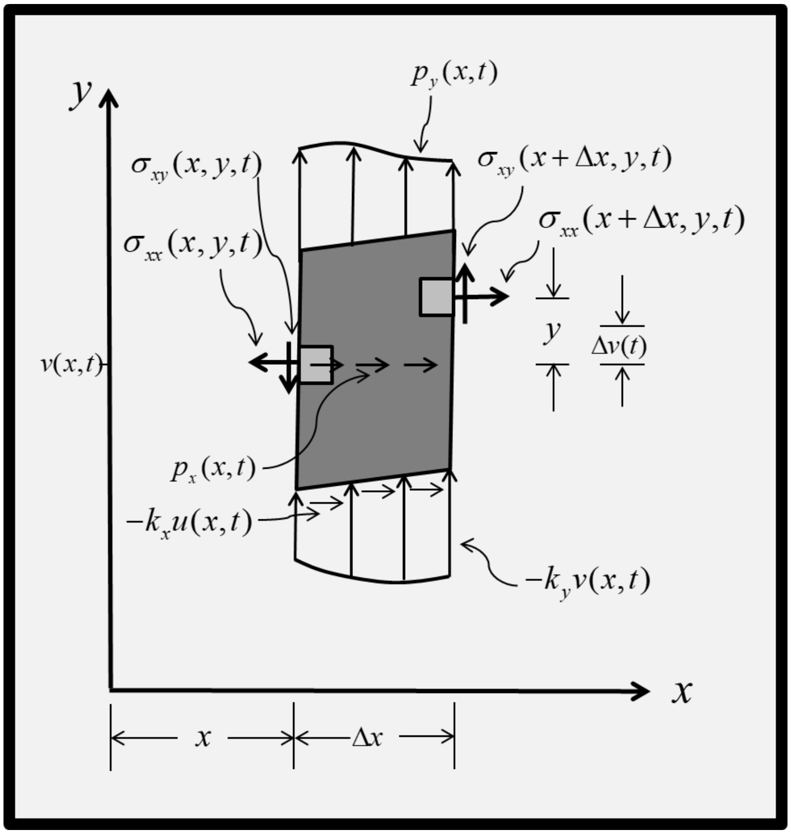

Figure 4. Top View of Free Body Diagram of Cut Rail (Reprinted with Permission from Musu 2021)

Note also that the stress components on the two vertical cuts within the rail are denoted generically by the two infinitesimal stress boxes on these faces. Finally, note that the differential element is depicted in the deformed configuration, so that the axial force affects the transverse displacement of the rail. This necessarily causes the response of the rail to be geometrically nonlinear.

A side view of a free body diagram of a section of the rail is constructed in Fig. 5, wherein the load per unit length applied to the centroidal axis of the rail is composed of components $p_x(x,t)$ and $p_z(x,t)$ in the *x* and *z* coordinate directions, respectively. In addition, the out-of-plane component of force per unit length applied to the bottom of the rail due to the out-of-plane displacement component w(x,t) is denoted as $-k_z w(x,t)$, where $k_z(x,t)$ is the track modulus and the negative sign is employed so that the base stiffness is non-negative when the resultant is positive due to downward displacement of the rail. Note that the side view is depicted in the undeformed configuration, therefore obviating the possibility of predicting out-of-plane (vertical) buckling of the rail. This simplification of the model results from the fact that the substantial difference in the second area moment of the rail about the x-y plane is sufficiently large to obviate out-of-plane buckling of the rail.

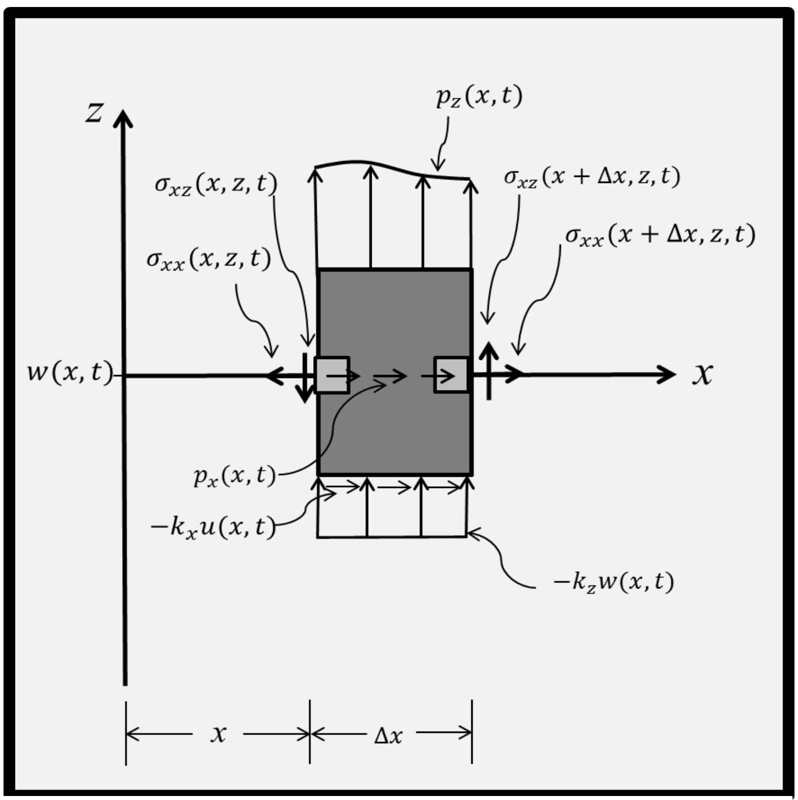

Figure 5. Side View of Free Body Diagram of Cut Rail (Reprinted with Permission from Musu 2021)

Consistent with Euler-Bernoulli beam theory the force and moment resultants in the x-y and x-z planes are now defined as follows (Allen and Haisler 1985):

$$P = P(x,t) \equiv \int_A \sigma_{xx} dA \tag{1}$$

$$V_y = V_y(x,t) \equiv \int_A \sigma_{xy} dA \tag{2}$$

$$V_z = V_z(x,t) \equiv \int_A \sigma_{xz} dA \tag{3}$$

$$M_y = M_y(x,t) \equiv \int_A \sigma_{xx} \bar{z} dA \tag{4}$$

$$M_z = M_z(x,t) \equiv -\int_A \sigma_{xx} \bar{y} dA \tag{5}$$

where A is the cross-sectional area of the rail, $\bar{y}$ is the horizontal distance from the centroid, and $\bar{z}$ is the vertical distance from the centroid. The resultants defined in equations (1)-(5) can be utilized to replace the stress components, so that the free body diagrams shown in Fig. 6 and Fig. 7 can be constructed.

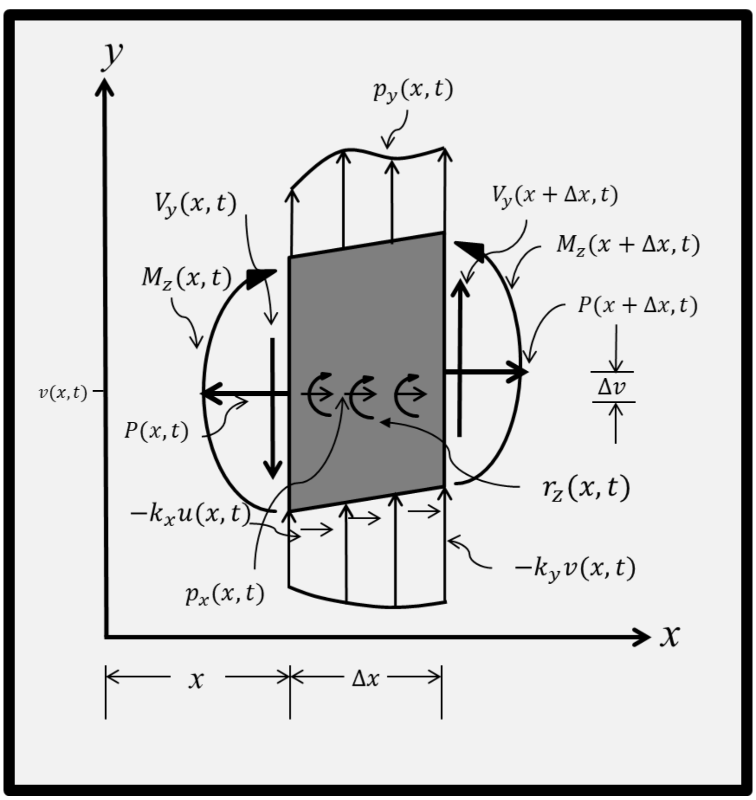

Figure 6. Resultant Forces and Moments Applied to a Differential Element of the Rail in the Horizontal Plane (Reprinted with Permission from Musu 2021)

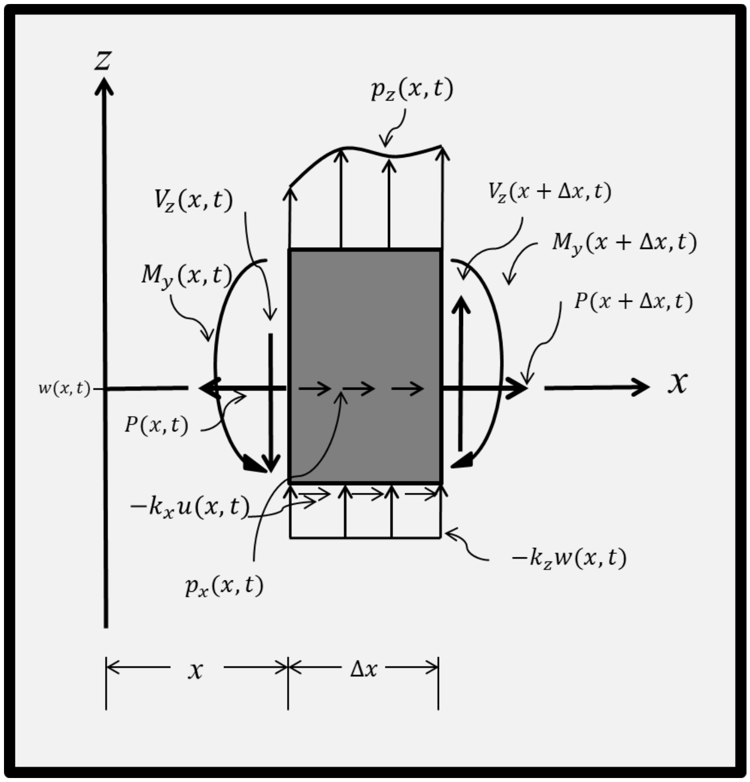

Figure 7. Resultant Forces and Moments Applied to a Differential Element of the Rail in the Vertical Plane (Reprinted with Permission from Musu 2021)

Note that the rotational resistance per unit length, $r_z(x,t)$, has been included in the free body diagram shown in Fig. 6. This resistance, due to the crosstie and fastener resistance to the rotation of the track, was previously introduced by Grissom and Kerr (Grissom and Kerr 2006). The inclusion of this term is explained by the fact that since the ballast and the fasteners impede rigid-body rotation of the crossties with the track, the crossties apply a moment in the opposite direction from the rotation of the track about the z-axis, and this moment is applied to the rail by the fastener connections. These moments are therefore pointwise in nature, but are depicted as distributed moments per unit length, $r_z(x,t)$, as a simplification to the model. This aspect of the model has the advantage that it captures the physical effects of the crossties on the rail response without actually requiring the crossties to be included as structural members, a complicating factor that has been reported elsewhere (Lim et al. 2003).

Assuming linear thermoelastic behavior, the axial stress within the rail is given by the following constitutive equation:

$$\sigma_{xx} = E(\varepsilon_{xx} - \alpha \Delta T) \tag{6}$$

where E is the modulus of elasticity of the rail, ε_{xx} is the axial strain within the rail, α is the coefficient of thermal expansion within the rail, and ΔT is the temperature change from the rail neutral temperature, which is assumed to be temporally variable, but spatially constant in the current dissertation. In addition, as shown in Figs. 8 and 9, the Euler-Bernoulli assumption that plane sections remain plane during the deformations results in the following kinematic relationship (Allen and Haisler 1985):

$$u(x,y) = u(x,0) - \theta_z(x)\bar{y} + \theta_y(x)\bar{z} \tag{7}$$

where $u(x,0)$ is the axial displacement of the real neutral surface, which will be denoted throughout the remainder of this paper simply as $u(x)$, $\theta_y = -\frac{dw}{dx}$ is the rotation of the rail neutral surface about the y coordinate axis and $\theta_z = \frac{dv}{dx}$ is the rotation of the rail neutral surface about the z coordinate axis.

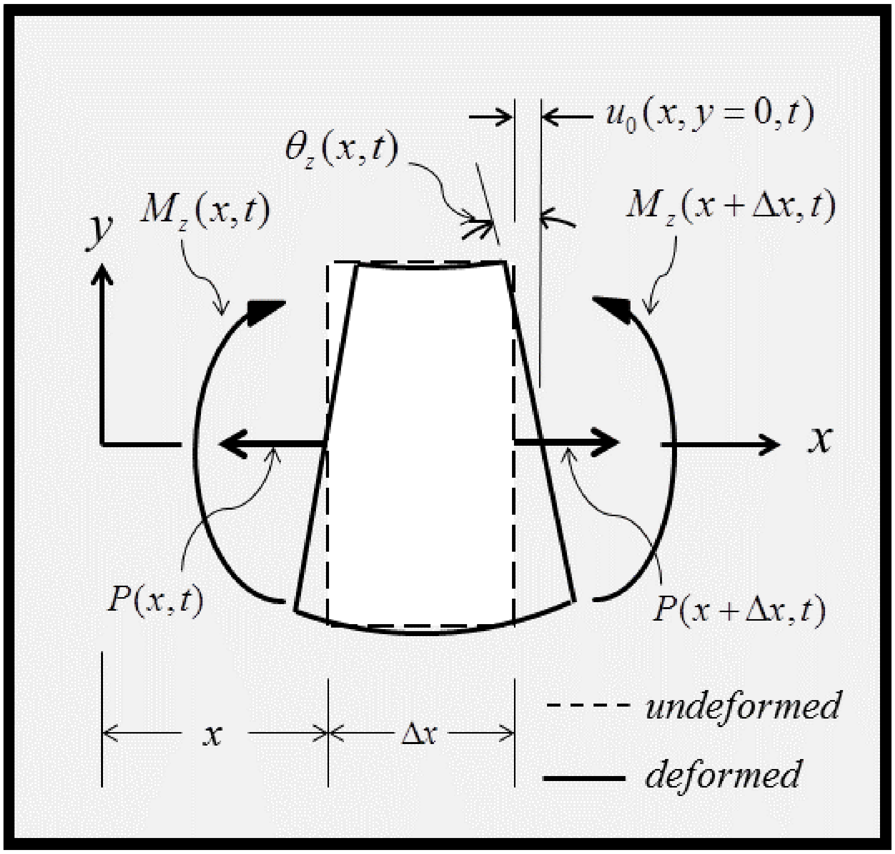

Figure 8. Depiction of the Kinematics of Displacement in a Euler-Bernoulli Beam in the Horizontal Plane (Reprinted with Permission from Musu 2021)

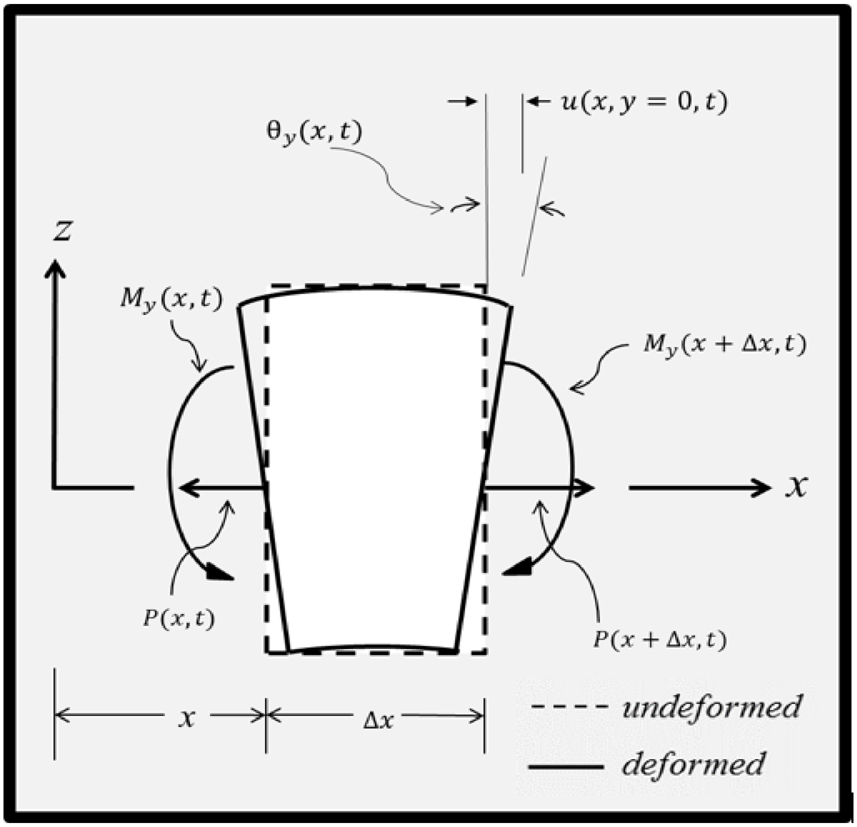

Figure 9. Depiction of the Kinematics of Displacement in a Euler-Bernoulli Beam in the Vertical Plane (Reprinted with Permission from Musu 2021)

Furthermore, the axial strain is approximated by (Tvergaard and Needleman 1981, Grissom and Kerr 2006):

$$\varepsilon_{xx} = \frac{du}{dx} + \frac{1}{2}\left(\frac{dv}{dx}\right)^2 \tag{8}$$

Note that it was assumed that the out-of-plane component of the displacement might be significant, however, it was assumed that $\frac{1}{2}\left(\frac{dw}{dx}\right)^2 \cong 0$. While the out-of-plane component is significant, it is still appropriate to assume small displacements in the vertical plane.

This is due to the geometry of the typical rail cross-section, whereas I_{yy} tends to be quite large, which is also a sufficient condition to obviate out-of-plane buckling in rails.

Substituting equation (7) into equation (8), and equation (6) into this result gives the following:

$$\sigma_{xx} = E\left[\frac{du}{dx} - \bar{y}\frac{d\theta_z}{dx} + \bar{z}\frac{d\theta_y}{dx} + \frac{1}{2}\left(\frac{dv}{dx}\right)^2 - \alpha\Delta T\right] \tag{9}$$

In addition, it is assumed that the relation between the rotational stiffness and the track rotation is given by the following constitutive relation:

$$r_z = -S\theta_z \tag{10}$$

Note that in the above equation it is assumed that the relation between the rotation of the track structure about the z coordinate axis and the angle of rotation is linear (Grissom and Kerr 2006). Whereas limited experimental data support this assumption (Grissom and Kerr 2006), it is to be noted that the rotational stiffness, S, depends strongly on the type of fastener used (Grissom and Kerr 2006). Furthermore, in the current research it will be assumed that S depends not only on the type of fasteners connecting the track to the crossties, but it is also a weak function of the number of cycles of loading, n_c, previously applied to the truck structure. Thus, at any point in time the relationship described by equation (10) is assumed to apply, but the value of S is at that point in time a constant depending on both the type of fasteners deployed and n_c, thereby quasi-linearizing this effect on the rail response. This assumption is based on anecdotal observation suggesting that the ballast settlement, grinding, spallation and rearrangement over time can affect the rotational resistance of the crosstie-fastener system to track rotation, and such an assumption will be validated experimentally in future research.

Applying Newton's first law to the forces in the x coordinate direction and moments about the y and z axis in Fig. (6) and (7) together with equations (1)-(10) will result in the general three-dimensional formulation shown in Table 1 for a generic rail subjected to mechanical and spatially constant thermal loading (Kerr 1974, 1978, Allen and Haisler 1985).

Table 1. Model for Predicting the Rail Response

Independent Variables: x, t

Known Inputs:

Loads: $p_x = p_x(x,t),\ p_y = p_y(x,t),\ p_z = p_z(x,t) \quad 0 < x < L$

Temperature change: $\Delta T = \Delta T(t) = known$

Geometry: $A, I_{yy}, I_{zz}, L, \bar{y}, \bar{z}$

Material Properties: $\alpha, E, k_x, k_y, k_z, S$

Unknowns: $u, v, w, \sigma_{xx}, P, V_y, V_z, M_y, M_z$ = **9 unknowns**

Field Equations:

	Equation	No. of Equations
(11)	$\frac{dP}{dx} = -p_x + k_x u$	1
(12)	$\frac{dV_y}{dx} = -p_y + k_y v$	1
(13)	$\frac{dV_z}{dx} = -p_z + k_z w$	1
(14)	$\frac{dM_y}{dx} = V_z$	1
(15)	$\frac{dM_z}{dx} = -V_y - (S - P)\frac{dv}{dx}$	1
(16)	$\frac{du}{dx} = \frac{(P+P^T)}{EA} - \frac{1}{2}\left(\frac{dv}{dx}\right)^2$	1
(17)	$\frac{d^2w}{dx^2} = -\frac{M_y}{EI_{yy}}$	1
(18)	$\frac{d^2v}{dx^2} = \frac{M_z}{EI_{zz}}$	1
(19)	$\sigma_{xx} = \frac{(P+P^T)}{A} - \frac{M_z\bar{y}}{I_{zz}} + \frac{M_y\bar{z}}{I_{yy}} - E\alpha\Delta T$	1
	Total	**9**

where it should be noted that all variables are defined in the Nomenclature Section of this manuscript.

It should be apparent that the problem formulated in Table 1 represents a well-posed boundary value problem when appropriate boundary conditions are imposed. However, as there are 9 coupled equations in 9 unknowns, it might be exceedingly difficult to solve, depending on the loading conditions and the material properties involved. In particular, the friction coefficients k_x and k_y are observed to be nonlinear, whereas k_z was assumed to behave linearly. Accordingly, although at least one solution has in fact been obtained for specialized, simplified conditions (Grissom and Kerr 2006), closed-form solutions are difficult to obtain for this problem. Note that while Grissom and Kerr proposed an analytical solution, a great number of simplifying assumptions had to be imposed in order to obtain it, thus significantly compromising the accuracy of the predicted results. Alternatively, computational solutions are possible using the finite element method, and this approach will be the subject of the next chapter.

CHAPTER III

VARIATIONAL FORMULATION*

In the present research the displacement components $u(x)$, $\mathrm{v}(x)$ and $w(x)$ are treated as primary unknowns. From equation (9) it can be seen that once these are determined the actual stress components follow quite simply, and the remaining unknowns can be calculated using equation (1)-(5). In order to construct a finite element algorithm for predicting the primary unknowns it is first necessary to construct a variational principle in terms of these unknowns. Briefly, this is accomplished by reducing out all the secondary unknowns according to equations (11), (12), (14)-(16) and (18) and integrating by parts all the higher order terms. This standard procedure allows the user to construct the so-called "weak form" of the original differential equations. The weak formulation has the advantages of weakening the continuity of the dependent variables, thus producing symmetric coefficient matrices, as well as including in the weak form the natural boundary conditions of the problem, which is performed to include physically meaningful boundary conditions for the problem. Both of these features help in the development of the finite element formulation of a problem (Reddy 1984, Oden 1972).

The weak formulation was derived in detail by Musu (Musu 2021) and the final form of the variational principle to be implemented within the finite element method (FEM) is reported in Equation (20).

*Partially reproduced with permission from the author, "*Computational Model for Predicting Buckling in Rail Structures*" by Valentina Musu [2021], An unpublished Master's Thesis, Texas A&M University

$$\int_0^L EA\frac{du}{dx}\delta\left(\frac{du}{dx}\right)dx + \int_0^L \left(EI_{zz}\frac{d^2v}{dx^2}\right)\delta\left(\frac{d^2v}{dx^2}\right)dx + \int_0^L \left(EI_{yy}\frac{d^2w}{dx^2}\right)\delta\left(\frac{d^2w}{dx^2}\right)dx +$$

$$-\int_0^L(-S + P^T)\frac{dv}{dx}\delta\left(\frac{dv}{dx}\right)dx + \int_0^L EA\frac{du}{dx}\frac{dv}{dx}\delta\left(\frac{dv}{dx}\right)dx + \int_0^L \frac{EA}{2}\left(\frac{dv}{dx}\right)^2\delta\left(\frac{du}{dx}\right)dx +$$

$$+\int_0^L \frac{EA}{2}\left(\frac{dv}{dx}\right)^3\delta\left(\frac{dv}{dx}\right)dx + \int_0^L k_x u\delta u\,dx + \int_0^L k_y v\delta v\,dx + \int_0^L k_z w\delta w\,dx =$$

$$\int_0^L p_x\delta u\,dx + \int_0^L P^T\,\delta\left(\frac{du}{dx}\right)dx + \int_0^L p_y\delta v\,dx + \int_0^L p_z\delta w\,dx + [(P\delta u)]_0^L + \left[V_y\delta v\right]_0^L +$$

$$[V_z\delta w]_0^L + \left[M_y\delta\theta_y\right]_0^L + [M_z\delta\theta_z]_0^L \qquad (20)$$

The above is utilized in the following chapter for the development of the finite element formulation.

CHAPTER IV

THE FINITE ELEMENT FORMULATION*

Equation (20) may now be discretized for a generic beam element in five degrees of freedom (DOF). To do this, it is assumed that, within a generic element of length, L_e, the displacement field may be approximated by complete algebraic polynomials that fulfill the following conditions (Reddy 1984, Allen and Haisler 1985):

1. The polynomials should be continuous and differentiable over the element in order to ensure nonzero coefficient matrices
2. The polynomials should be complete so that all possible states of the solution might be captured (i.e. constant, linear etc.)
3. The polynomial should be an interpolant of the primary variables at the nodes of the element in order to enforce continuity of the solution across common nodes

The assumed displacement field and shape functions were reported in detail by Musu (Musu 2021) and may be substituted into the variational principle (20), thereby resulting in algebraic equations of the following form for a generic frame element (Reddy 1984, Allen and Haisler 1985):

$$\sum_{j=1}^{10} K_{ij}^e\, q_j^e + \sum_{j=1}^{10} B_{ij}^e\, q_j^e + \sum_{j=1}^{10} G_{ij}^e\, q_j^e + \sum_{j=1}^{10} H_{ij}^e\, q_j^e + \sum_{j=1}^{10} M_{ij}^e\, q_j^e + \sum_{j=1}^{10} N_{ij}^e\, q_j^e = F_i^e$$

$$i = 1, \dots 10 \qquad (21)$$

where each term above accounts for one or more terms in equation (20) as reported by Musu (Musu 2021). Furthermore, note that nonlinear matrices H_{ij}^e and M_{ij}^e presented in equation (21) will be neglected in the implementation of this model under the assumption that linear small strain theory is sufficient to accurately predict lateral buckling in rails. In addition,

$$\{q_j^e\} \equiv \begin{Bmatrix} u_1^e \\ v_1^e \\ w_1^e \\ \theta_{y1}^e \\ \theta_{z1}^e \\ u_2^e \\ v_2^e \\ w_2^e \\ \theta_{y2}^e \\ \theta_{z2}^e \end{Bmatrix} \tag{22}$$

where u_1^e and u_2^e are the axial displacement components at the left and right ends of element *e,* v_1^e, v_2^e, $w_1^e$and w_2^e are respectively the lateral and vertical displacement components at the left and right ends of element *e*, and θ_{y1}^e, θ_{y2}^e, θ_{z1}^e and θ_{z2}^e are respectively, the rotation components about the y and z axes at the left and right ends of element *e*. Moreover,

$$[K^e] = \begin{bmatrix} \frac{E^eA^e}{L^e} & 0 & 0 & 0 & 0 & -\frac{E^eA^e}{L^e} & 0 & 0 & 0 & 0 \\ 0 & \frac{12E^eI_{zz}^e}{(L^e)^3} & 0 & 0 & \frac{6E^eI_{zz}^e}{(L^e)^2} & 0 & -\frac{12E^eI_{zz}^e}{(L^e)^3} & 0 & 0 & \frac{6E^eI_{zz}^e}{(L^e)^2} \\ 0 & 0 & \frac{12E^eI_{yy}^e}{(L^e)^3} & -\frac{6E^eI_{yy}^e}{(L^e)^2} & 0 & 0 & 0 & -\frac{12E^eI_{yy}^e}{(L^e)^3} & -\frac{6E^eI_{yy}^e}{(L^e)^2} & 0 \\ 0 & 0 & -\frac{6E^eI_{yy}^e}{(L^e)^2} & \frac{4E^eI_{yy}^e}{L^e} & 0 & 0 & 0 & \frac{6E^eI_{yy}^e}{(L^e)^2} & \frac{2E^eI_{yy}^e}{L^e} & 0 \\ 0 & \frac{6E^eI_{zz}^e}{(L^e)^2} & 0 & 0 & \frac{4E^eI_{yy}^e}{L^e} & 0 & -\frac{6E^eI_{zz}^e}{(L^e)^2} & 0 & 0 & \frac{2E^eI_{zz}^e}{L^e} \\ -\frac{E^eA^e}{L^e} & 0 & 0 & 0 & 0 & \frac{E^eA^e}{L^e} & 0 & 0 & 0 & 0 \\ 0 & -\frac{12E^eI_{zz}^e}{(L^e)^3} & 0 & 0 & -\frac{6E^eI_{zz}^e}{(L^e)^2} & 0 & \frac{12E^eI_{zz}^e}{(L^e)^3} & 0 & 0 & -\frac{6E^eI_{zz}^e}{(L^e)^2} \\ 0 & 0 & -\frac{12E^eI_{yy}^e}{(L^e)^3} & \frac{6E^eI_{yy}^e}{(L^e)^2} & 0 & 0 & 0 & \frac{12E^eI_{yy}^e}{(L^e)^3} & \frac{6E^eI_{yy}^e}{(L^e)^2} & 0 \\ 0 & 0 & -\frac{6E^eI_{yy}^e}{(L^e)^2} & \frac{2E^eI_{yy}^e}{L^e} & 0 & 0 & 0 & \frac{6E^eI_{yy}^e}{(L^e)^2} & \frac{4E^eI_{yy}^e}{L^e} & 0 \\ 0 & \frac{6E^eI_{zz}^e}{(L^e)^2} & 0 & 0 & \frac{2E^eI_{zz}^e}{L^e} & 0 & -\frac{6E^eI_{zz}^e}{(L^e)^2} & 0 & 0 & \frac{4E^eI_{zz}^e}{L^e} \end{bmatrix} \quad (23)$$

Furthermore, for linearly varying distributed lateral and vertical loads given by:

$$p_y(\bar{x}) = p_y^0 + (p_y^{L^e} - p_y^0)\frac{\bar{x}}{L^e}$$

$$p_z(\bar{x}) = p_z^0 + (p_z^{L^e} - p_z^0)\frac{\bar{x}}{L^e} \quad (24)$$

$$\{F^e\} = \begin{Bmatrix} \frac{p_xL^e}{2} - E^eA^e\alpha^e\Delta T^e \\ \frac{p_y^0L^e}{2} + \frac{3L^e}{20}\left(p_y^{L^e} - p_y^0\right) \\ \frac{p_z^0L^e}{2} + \frac{3L^e}{20}\left(p_z^{L^e} - p_z^0\right) \\ -\frac{p_z^0(L^e)^2}{12} - \frac{(L^e)^2}{30}\left(p_z^{L^e} - p_z^0\right) \\ \frac{p_y^0(L^e)^2}{12} + \frac{(L^e)^2}{30}\left(p_y^{L^e} - p_y^0\right) \\ \frac{p_xL^e}{2} + E^eA^e\alpha^e\Delta T^e \\ \frac{p_y^0L^e}{2} + \frac{7L^e}{20}\left(p_y^{L^e} - p_y^0\right) \\ \frac{p_z^0L^e}{2} + \frac{7L^e}{20}\left(p_z^{L^e} - p_z^0\right) \\ \frac{p_z^0(L^e)^2}{12} + \frac{(L^e)^2}{20}\left(p_z^{L^e} - p_z^0\right) \\ -\frac{p_y^0(L^e)^2}{12} - \frac{(L^e)^2}{20}\left(p_y^{L^e} - p_y^0\right) \end{Bmatrix} \quad (25)$$

Note that the interelement boundary terms are not included because they will cancel one another when the global equations are assembled. Additionally, when the second through sixth terms in equation (21) may be neglected, the standard finite element formulation for a linear thermoelastic beam undergoing small displacements is recovered. However, in the current case it remains to account for all of the remaining terms presented in equation (20) or (21).

Consider first the fourth term in equation (20) This term is given by:

$$\{B^e\} = -(-S + P^T)\begin{bmatrix} 0 & 0 & 0 & 0 & 0 & 0 & 0 & 0 & 0 & 0 \\ 0 & \frac{6}{5L^e} & 0 & 0 & 0.10 & 0 & -\frac{6}{5L^e} & 0 & 0 & 0.10 \\ 0 & 0 & 0 & 0 & 0 & 0 & 0 & 0 & 0 & 0 \\ 0 & 0 & 0 & 0 & 0 & 0 & 0 & 0 & 0 & 0 \\ 0 & 0.10 & 0 & 0 & \frac{2L^e}{15} & 0 & -0.10 & 0 & 0 & -\frac{L^e}{30} \\ 0 & 0 & 0 & 0 & 0 & 0 & 0 & 0 & 0 & 0 \\ 0 & -\frac{6}{5L^e} & 0 & 0 & -0.10 & 0 & \frac{6}{5L^e} & 0 & 0 & -0.10 \\ 0 & 0 & 0 & 0 & 0 & 0 & 0 & 0 & 0 & 0 \\ 0 & 0 & 0 & 0 & 0 & 0 & 0 & 0 & 0 & 0 \\ 0 & 0.10 & 0 & 0 & -\frac{L^e}{30} & 0 & -0.10 & 0 & 0 & \frac{2L^e}{15} \end{bmatrix} \tag{26}$$

Now consider the fifth term in equation (20). This term is nonlinear, being first order in both $u(x)$ and $v(x)$ at any point in time. In the case wherein it is sufficiently accurate to assume that $u(x, t + \Delta t)$ may be approximated by the values of the previous step, $u(x, t)$, the result is as follows:

$$\{G^e(t+\Delta t)\} = EA\left(\frac{u_2^e(t)-u_1^e(t)}{L^e}\right)\begin{bmatrix} 0 & 0 & 0 & 0 & 0 & 0 & 0 & 0 & 0 & 0 \\ 0 & \frac{6}{5L^e} & 0 & 0 & 0.10 & 0 & -\frac{6}{5L^e} & 0 & 0 & 0.10 \\ 0 & 0 & 0 & 0 & 0 & 0 & 0 & 0 & 0 & 0 \\ 0 & 0 & 0 & 0 & 0 & 0 & 0 & 0 & 0 & 0 \\ 0 & 0.10 & 0 & 0 & \frac{2L^e}{15} & 0 & -0.10 & 0 & 0 & -\frac{L^e}{30} \\ 0 & 0 & 0 & 0 & 0 & 0 & 0 & 0 & 0 & 0 \\ 0 & -\frac{6}{5L^e} & 0 & 0 & -0.10 & 0 & \frac{6}{5L^e} & 0 & 0 & -0.10 \\ 0 & 0 & 0 & 0 & 0 & 0 & 0 & 0 & 0 & 0 \\ 0 & 0 & 0 & 0 & 0 & 0 & 0 & 0 & 0 & 0 \\ 0 & 0.10 & 0 & 0 & -\frac{L^e}{30} & 0 & -0.10 & 0 & 0 & \frac{2L^e}{15} \end{bmatrix} \quad (27)$$

Now consider the eighth, ninth and tenth terms in equation (20). In the case wherein it is sufficiently accurate to assume that the coefficients of friction, k_x and k_y vary linearly in *x* in each element, the result is as follows:

$$[N^e] = \begin{bmatrix} A & B \\ C & D \end{bmatrix} \quad (28)$$

where,

$[A] =$

$$\begin{bmatrix} \frac{k_x^L L_e}{3} + \frac{(k_x^R - k_x^L)L_e}{12} & 0 & 0 & 0 & 0 \\ 0 & \frac{13k_y^L L_e}{35} + \frac{3(k_y^R - k_y^L)L_e}{35} & 0 & 0 & \frac{11k_y^L (L_e)^2}{210} + \frac{(k_y^R - k_y^L)(L_e)^2}{60} \\ 0 & 0 & \frac{13k_z L_e}{35} & -\frac{11k_z (L_e)^2}{210} & 0 \\ 0 & 0 & -\frac{11k_z (L_e)^2}{210} & \frac{k_z (L_e)^3}{105} & 0 \\ 0 & \frac{11k_y^L (L_e)^2}{210} + \frac{(k_y^R - k_y^L)(L_e)^2}{60} & 0 & 0 & \frac{k_y^L (L_e)^3}{105} + \frac{(k_y^R - k_y^L)(L_e)^3}{280} \end{bmatrix}$$

$[B] =$

$$\begin{bmatrix} \frac{k_x^L L_e}{6} + \frac{(k_x^R - k_x^L) L_e}{12} & 0 & 0 & 0 & 0 \\ 0 & \frac{9 k_y^L L_e}{70} + \frac{9(k_y^R - k_y^L) L_e}{140} & 0 & 0 & -\frac{13 k_y^L (L_e)^2}{420} - \frac{(k_y^R - k_y^L)(L_e)^2}{70} \\ 0 & 0 & \frac{9 k_z L_e}{70} & \frac{13 k_z (L_e)^2}{420} & 0 \\ 0 & 0 & \frac{13 k_z (L_e)^2}{420} & -\frac{k_z (L_e)^3}{140} & 0 \\ 0 & \frac{13 k_y^L (L_e)^2}{420} + \frac{(k_y^R - k_y^L)(L_e)^2}{60} & 0 & 0 & -\frac{k_y^L (L_e)^3}{140} - \frac{(k_y^R - k_y^L)(L_e)^3}{280} \end{bmatrix}$$

$[C] =$

$$\begin{bmatrix} \frac{k_x^L L_e}{6} + \frac{(k_x^R - k_x^L) L_e}{12} & 0 & 0 & 0 & 0 \\ 0 & \frac{9 k_y^L L_e}{70} + \frac{9(k_y^R - k_y^L) L_e}{140} & 0 & 0 & \frac{13 k_y^L (L_e)^2}{420} + \frac{(k_y^R - k_y^L)(L_e)^2}{60} \\ 0 & 0 & \frac{9 k_z L_e}{70} & -\frac{13 k_z (L_e)^2}{420} & 0 \\ 0 & 0 & -\frac{13 k_z (L_e)^2}{420} & \frac{k_z (L_e)^3}{140} & 0 \\ 0 & -\frac{13 k_y^L (L_e)^2}{420} - \frac{(k_y^R - k_y^L)(L_e)^2}{70} & 0 & 0 & -\frac{k_y^L (L_e)^3}{140} - \frac{(k_y^R - k_y^L)(L_e)^3}{280} \end{bmatrix}$$

$[D] =$

$$\begin{bmatrix} \frac{k_x^L L_e}{3} + \frac{(k_x^R - k_x^L) L_e}{4} & 0 & 0 & 0 & 0 \\ 0 & \frac{13 k_y^L L_e}{35} + \frac{2(k_y^R - k_y^L) L_e}{7} & 0 & 0 & -\frac{11 k_y^L (L_e)^2}{210} - \frac{(k_y^R - k_y^L)(L_e)^2}{28} \\ 0 & 0 & \frac{13 k_z L_e}{35} & \frac{11 k_z (L_e)^2}{210} & 0 \\ 0 & 0 & \frac{11 k_z (L_e)^2}{210} & \frac{k_z (L_e)^3}{105} & 0 \\ 0 & -\frac{11 k_y^L (L_e)^2}{210} - \frac{(k_y^R - k_y^L)(L_e)^2}{28} & 0 & 0 & \frac{k_y^L (L_e)^3}{105} + \frac{(k_y^R - k_y^L)(L_e)^3}{168} \end{bmatrix}$$

And,

$$k_x(x) = k_x^L + (k_x^R - k_x^L)\frac{x}{L_e}$$

$$k_y(x) = k_y^L + (k_y^R - k_y^L)\frac{x}{L_e}$$

$$k_z(x) = k_z = const. \tag{29}$$

where in addition $k_{x,y}^L$ and $k_{x,y}^R$ are the values of the axial and lateral coefficients of friction at $x = [0, L_e]$ within the element e and k_z is the elastic modulus of the foundation (or track modulus) within the element e. Note that in assuming that the axial and lateral coefficients of friction, k_x and k_y, vary linearly within the element, necessarily results in a nonlinear coefficient matrix. The nonlinearity enters via the dependence of the friction coefficients on the displacement components, $u(x)$ and $v(x)$, respectively, as shown in detail in Chapter V. Finally, in the case where it is sufficiently accurate to assume that the friction, k_x and k_y are constant in *x* in each element, the linear form of equation (28) can be recovered by satisfying the following conditions:

$$k_x(x) = k_x^R = k_x^L = k_x = const.$$

$$k_y(x) = k_y^R = k_y^L = k_y = const. \tag{30}$$

The above element equations may be assembled into a global finite element formulation using the standard assembly technique (Reddy 1984 and 2005), and this has been accomplished by the authors. This then completes the finite element formulation.

Now consider the fifth term in equation (20) once again. The fifth term is nonzero and therefore nonlinear whenever there is axial displacement. Finally, consider the eighth and ninth terms in equation (20). These terms will necessarily be nonlinear whenever the coefficients of friction, k_x and k_y, are not constant, and this circumstance is the main purpose of the current study. Accordingly, failing to account for the nonlinearity in the model can lead to significant predictive error. Therefore, it is essential to include the ability to predict this nonlinearity in the model (Tvergaard and Needleman 1981, Lim et al. 2003, Grissom and Kerr 2006, Allen et al 2006). Toward this end, a standard time marching scheme is adopted herein, in which the externally applied mechanical load is gradually increased in a series of time steps, with Newton iteration deployed to capture the nonlinearity on each time step (Little et al. 2016).

Briefly, this is accomplished by first obtaining an approximate solution in which it is assumed that in the nonlinear terms the displacement from the previous time step is used, thereby resulting in the following initial approximation for the global form of equation (21).

$$\sum_{j=1}^{10} K_{ij}\,\Delta q_j^0 + \sum_{j=1}^{10} B_{ij}\,\Delta q_j^0 + \sum_{j=1}^{10} G_{ij}\,\Delta q_j^0 + \sum_{j=1}^{10} N_{ij}\,\Delta q_j^0 = \Delta F_i \qquad (31)$$

This erroneous value of $\Delta u^m(x)$ and $\Delta v^m(x)$ can be utilized to reduce the error by employing the following simple iteration method:

$$\left(G_{ij}\right)^{\eta} = \left(G_{ij}(q_j^{\eta-1})\right)$$

$$\left(N_{ij}\right)^{\eta} = \left(N_{ij}(q_j^{\eta-1})\right) \tag{32}$$

where η is the iteration number (Ketter and Prawel 1969, Little et al. 2016). Equation (31) is then reevaluated using the updated estimate of the matrices G_{ij} and N_{ij} obtained from equation (32). The iterative process is terminated when the following condition is satisfied:

$$\frac{\left\| \Delta q_i^{\eta} - \Delta q_i^{\eta-1} \right\|}{\left\| \Delta q_i^{\eta} \right\|} \leq e_{AL} \tag{33}$$

where the double vertical lines signify the Euclidean norm, and e_{AL} is a preset value of allowable error. The total displacement field is subsequently evaluated as follows:

$$q_i(x(t + \Delta t)) = q_i(x(t)) + \Delta q_i^{\eta}(x(t + \Delta t)) \tag{34}$$

This then concludes the implementation of the model into a nonlinear finite element formulation.

VERIFICATION OF THE MODEL

The finite element algorithm presented herein was verified extensively through a series of example problems for cases where either exact or variational analytical solutions exist. The full verification of the code can be found in (Musu 2021), but two such cases are reported below.

Example Problem #1: Doubly Cantilevered Beam Subjected to Nonlinear Friction

Given: A double-cantilevered beam is subjected to a distributed loading, where E=2.06x10^{11} N/m^2, I_{yy}=I_{zz}=8.99x10^{-6} m^4, A=0.0145 m^2, l=12.0 m,$\alpha = 1.05x10^{-5}\ /°C$, $p_x = p_z = k_x = k_z = S = 0$ and $\Delta T = 50\ °C$. In addition, the lateral coefficient of friction parameters used to fit the data in Fig. 22 are $k_y^0 = 1.16x10^6 N/m^2$, $k_y^1 = 6.5x10^5 N/m^2$, $v_0 = 0.005\ m$ and n=0.05.

Required:

- **a)** Obtain an analytic solution for $v = v(x, p_y^0, E, I_{zz})$
- **b)** Obtain a solution using finite elements and compare the two

Solution:

a) The solution solves the following differential equation:

$$EI_{zz}\frac{d^4v}{dx^4} + P^T\frac{d^2v}{dx^2} + k_y v = p_y \tag{E1.1}$$

Suppose that we choose the following:

$$v(x) = C_1\left[x^2 - \frac{2x^3}{l} + \frac{x^4}{l^2}\right] \quad 0 \le x \le l \tag{E1.2}$$

where l is the length of the beam and C_1 is a loading constant. It can be seen that the above assumed solution satisfies the following boundary conditions:

$$v(x = 0, l) = 0$$

$$\frac{dv}{dx}(x = 0, l) = 0 \tag{E1.3}$$

In order to obtain the forcing function, p_y, equation (E1.2) is now substituted into equation (E1.1) and it is solved, thereby resulting in the following:

$$p_y(x) = C_1 EI_{zz}\frac{d^4}{dx^4}\left[x^2 - \frac{2x^3}{l} + \frac{x^4}{l^2}\right] + C_1 P^T\frac{d^2}{dx^2}\left[x^2 - \frac{2x^3}{l} + \frac{x^4}{l^2}\right] +$$

$$+ C_1\left[k_y^0 - k_y^1\left[\frac{C_1\left[x^2 - \frac{2x^3}{l} + \frac{x^4}{l^2}\right]}{v_0}\right]^n\right]\left[x^2 - \frac{2x^3}{l} + \frac{x^4}{l^2}\right] = \frac{24C_1 EI_{zz}}{l^2} +$$

$$+ C_1 P^T\left(2 - \frac{12x}{l} + \frac{12x^2}{l^2}\right) + C_1\left[k_y^0 - k_y^1\left[\frac{C_1\left[x^2 - \frac{2x^3}{l} + \frac{x^4}{l^2}\right]}{v_0}\right]^n\right]\left[x^2 - \frac{2x^3}{l} + \frac{x^4}{l^2}\right] \tag{E1.4}$$

The above forcing function will produce the displacement field given in equation (E1.2).

b) The next step is to compare the computational results obtained with the finite element algorithm to the exact solution represented by equations (E1.2) and (E1.4). Toward this end, an allowable error of $e_{AL} = 5.0X10^{-6}$ has been utilized. Fig. 10 shows the predicted vs. exact results for three different element meshes. On the basis of these results it is concluded that a 20-element mesh is sufficiently accurate for the purpose of approximating the displacement field within a rail structure modeled by equations (11)-(19). Furthermore, Fig. 11 shows the finite element predictions using the 20-element mesh and iterating through convergence at the last time step. On the basis of this, it is concluded that only a few iterations are necessary to accurately predict the effects of nonlinearity in the friction between the ballast-crosstie interface.

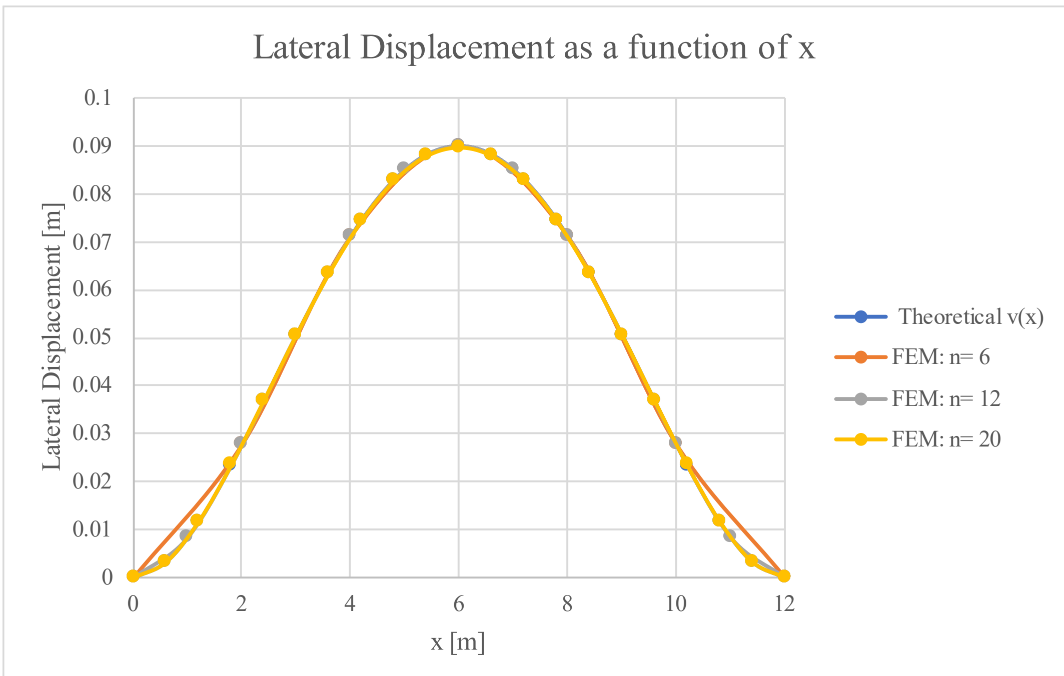

Figure 10. Comparison of Finite Element Approximations for Three Different Meshes to Theoretical Solution for Example Problem #1

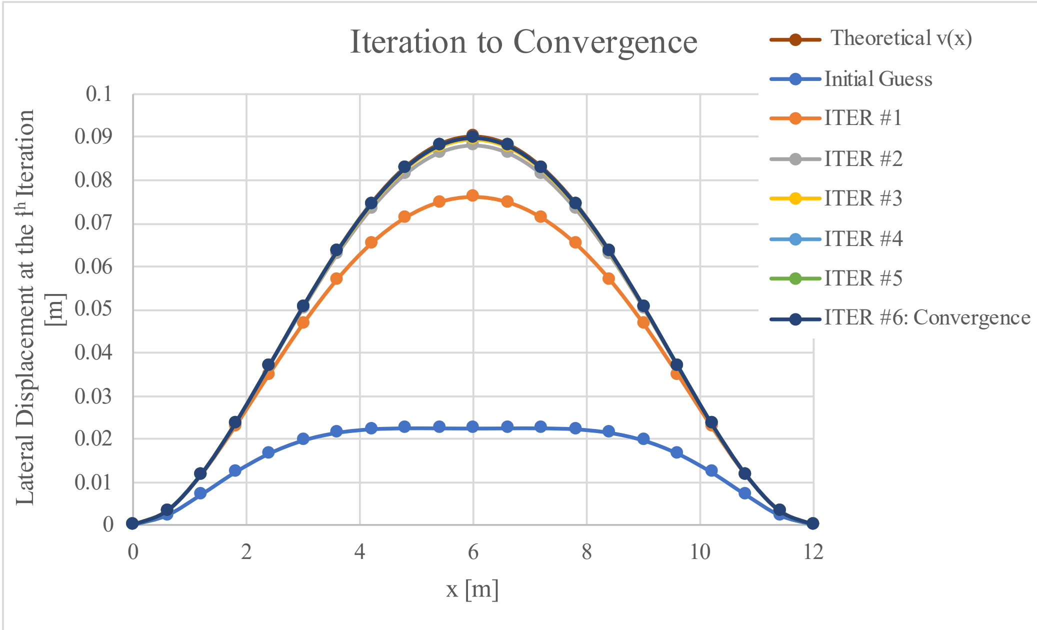

Figure 11. Comparison of Finite Element Approximations for Different Iterations (20 Element Mesh) to Theoretical Solution for Example Problem #1

Example Problem #2: Buckling of a Simply Supported Beam

Given: A beam that is simply supported at both ends is subjected to an incremental lateral distributed loading $p_y = const = 10\ N/m$, where E=2.06x10^{11} N/m^2, I_{yy}=I_{zz}=8.99x10^{-6} m^4, A=0.0145 m^2, l=12.0 m, and $p_x = p_z = k_x = k_y = k_z = S = \Delta T = 0$. The beam is subjected to an axial load, P, at the end x=0.

Required:

a) Obtain an approximate analytic solution for $v = v(x)$ and determine the axial load, P_{cr}, that will cause the column to buckle

b) Determine the location of the maximum lateral displacement and evaluate it

c) Obtain a solution using the finite element method and compare the two

Solution:

a) The analytic solution solves the following variational equation:

$$\int_0^l EI_{zz} \frac{d^2v}{dx^2} \delta\left(\frac{d^2v}{dx^2}\right) dx + \int_0^l P \frac{dv}{dx} \delta\left(\frac{dv}{dx}\right) dx - \int_0^l p_y \delta v dx = 0 \tag{E2.1}$$

The analytic solution is assumed to be of the following form:

$$v(x) = a_1 + a_2 x + a_3 x^2 \tag{E2.2}$$

It follows that

$$\frac{dv}{dx}(x) = a_2 + 2a_3 x \tag{E2.3}$$

where the coefficients are to be determined. The displacement boundary condition on the left end implies that:

$$v(x = 0) = 0 \Rightarrow a_1 = 0 \tag{E2.4}$$

Thus, equation (E2.2) simplifies to the following:

$$v(x) = a_2 x + a_3 x^2 \tag{E2.5}$$

The displacement boundary condition on the right end implies that

$$v(x = l) = 0 = a_2 l + a_3 l^2 \Rightarrow a_2 = -a_3 l \tag{E2.6}$$

Substituting (E2.6) into (E2.5) therefore results in:

$$v(x) = C(x^2 - xl) \tag{E2.7}$$

where the coefficient C is to be determined by satisfying (E2.1). Substituting (E2.7) into (E2.1) thus results in the following:

$$\left(4EI_{zz}lC + \tfrac{1}{3}Pl^3C + \tfrac{1}{6}l^3p_y\right)\delta C = 0 \tag{E2.8}$$

Since δC is arbitrary, it follows that

$$C = -\frac{p_y l^2}{6}\left[\frac{1}{\left(\frac{1}{3}Pl^2 + 4EI_{zz}\right)}\right] \tag{E2.9}$$

Substituting (E2.9) into (E2.7) gives the displacement field:

$$v(x) = -\frac{p_y l^2}{6}\left[\frac{1}{\left(\frac{1}{3}Pl^2 + 4EI_{zz}\right)}\right](x^2 - xl) \tag{E2.10}$$

To obtain the buckling load, the second variation of equation (E2.8) is taken, thereby resulting in the following:

$$\left(4EI_{zz}l + \tfrac{1}{3}P_{cr}l^3\right)\delta C = 0 \tag{E2.11}$$

Since δC is arbitrary, it follows that

$$P_{cr} = -12\frac{EI_{zz}}{l^2} \tag{E2.12}$$

b) The maximum lateral displacement can be seen to occur at the midpoint of the beam, so that:

$$v_{\max} = v(x = l/2) = \frac{p_y l^4}{24}\left[\frac{1}{\left(4EI_{zz} + \frac{1}{3}Pl^2\right)}\right] \tag{E2.13}$$

Note also that the end rotation can also be evaluated by differentiating equations (E2.13) as follows:

$$\theta(x) \equiv \frac{dv}{dx}(x) = -\frac{p_y l^2}{6}\left[\frac{1}{\left(\frac{1}{3}Pl^2 + 4EI_{zz}\right)}\right](2x - l) \tag{E2.14}$$

The predicted value of $\theta(x=0) = \theta_0$ can now be substituted into the above to obtain the following:

$$\theta_0 = \frac{p_y l^3}{6}\left[\frac{1}{\left(4EI_{zz} + \frac{1}{3}Pl^2\right)}\right] \tag{E2.15}$$

Substituting the above result back into equation (E2.13) thus gives the following:

$$v^{FE}_{\max} = \theta_0 l/4 \tag{E2.16}$$

c) In order to account for the coupling between the axial and lateral displacement components it is necessary to solve the problem with multiple elements using the finite element method. Fig. 12 shows the results of the finite element prediction using six elements of equal length, wherein it can be seen that the predicted maximum displacement buckling load match the results obtained above.

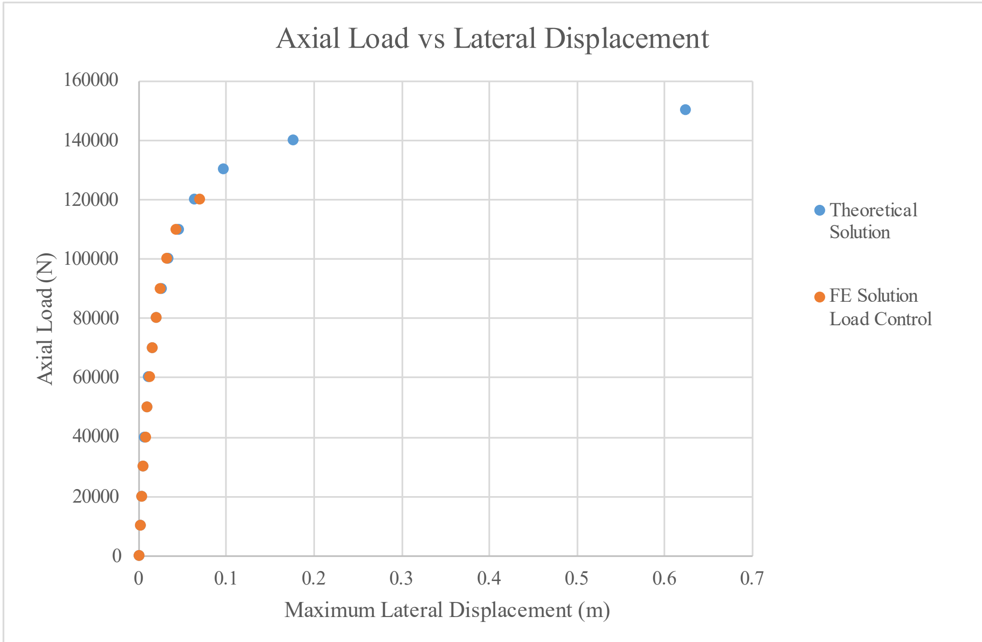

Figure 12. Comparison of Finite Element Approximation to Variational Solution for Example Problem #1

MODELING CONSIDERATIONS FOR BUCKLING PROBLEMS

The algorithm presented herein was developed with the goal of aiding the track engineer in the prediction of the onset of environmentally induced buckling in rail structures. For this purpose, it is therefore necessary to define the buckling load and in general, how to model buckling problems numerically.

In the above example problem, the load-displacement curve was generated for a simply supported beam subjected to lateral and axial loading. Since for this particular problem an analytical solution can be obtained, it was possible to determine the critical axial load as shown in equation (E2.12). This analytical expression then represents the buckling load for the specified set of loads, geometry and material properties, which is defined as the first local maximum of the load-displacement curve. Note however, that for most practical rail applications, analytical solutions to the governing equations cannot be obtained and therefore, it is still necessary to develop a protocol to model buckling problems and to appropriately define the buckling load that can be obtained numerically.

Noting once again that in order to capture the nonlinearity due to buckling for a given set of loads, geometry, material properties and boundary conditions, a standard time marching scheme was implemented by monotonically increasing the loading on the beam and obtaining a solution for the primary unknowns of the problem at each time step. This load-stepping, therefore, also allows for the load-displacement curve to be generated. Considering once again the load-displacement curve shown in Fig. 12, it can be seen that the finite element algorithm presented herein adequately and accurately predicts the lateral displacement at each load-step when compared to the obtained analytical solution. However, it is important to note that the numerical algorithm breaks down before reaching

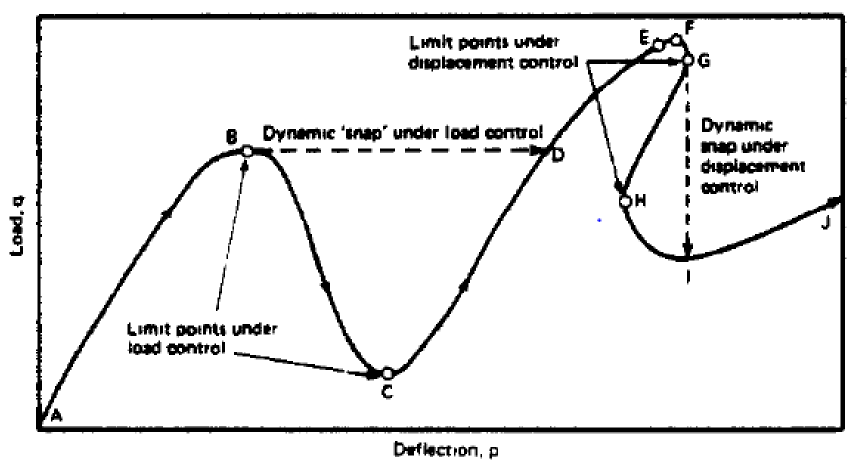

Figure 13. Depiction of the Deviation from the Equilibrium Path Under Load Control – Snapping (Crisfield 1981)

the critical point, thus slightly underpredicting the buckling load. This is a known shortcoming of the application of Newton's Iteration in load control, whereas a solution to the nonlinear system of equations can only be obtained up to the critical point. Fig. 13, below, illustrates the theoretical equilibrium path for a structure subjected to monotonically increasing loading. Point B in Fig. 13 represents the first local maximum which is defined as the buckling load of the structure. Past this critical point then the structure is known to first undergo softening and then successively hardening, generally referred to as post-buckling behavior. However, in load control the numerical scheme fails to accurately follow the equilibrium path once the neighborhood of the instability is reached. At this point then, the numerical prediction deviates from the equilibrium path and either snaps to the next equilibrium point, as illustrated by point D in Fig. 13, or bifurcates, as shown below in Fig. 14.

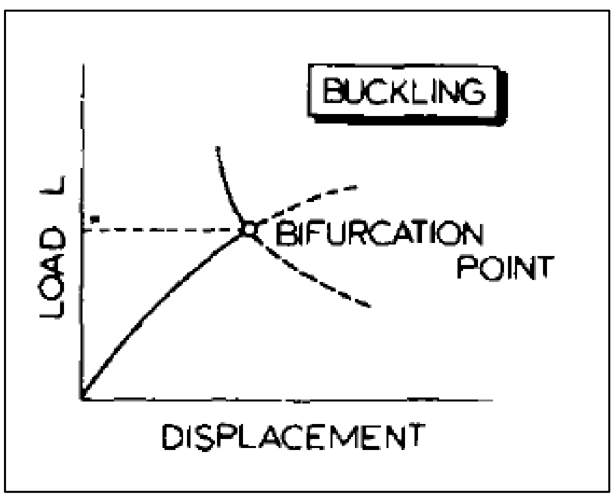

Figure 14. Depiction of the Deviation from the Equilibrium Path Under Load Control – Bifurcation Point (Riks1979)

Thus, the buckling load obtained numerically will be defined as the axial loading, either thermally or mechanically induced, applied on the structure at the last load step before the instability occurs. Table 2, shown below, illustrates the general procedure utilized to obtain the buckling load for a generic rail structure.

Table 2. General Procedure for Simulating Buckling Problems for a Generic Rail Structure

Initialization:

1) Turn on nonlinear and buckling control flags

2) Select time step size

3) Input loads, geometry, material properties and boundary conditions

4) Run the code and obtain output file

Post Processing:

1) Identify location of maximum lateral displacement

2) Record the maximum lateral displacement at each time step

3) Record the maximum axial load at each time step

4) Use the previous steps 2 and 3 to plot the load displacement curve

5) Identify the instability – either a snap through or a bifurcation point

6) Identify the buckling load as the axial load at the time step before the instability

Step Size Convergence:

1) Refine the step size and repeat the previous steps until the buckling load converges to at least two significant figures

CHAPTER V

SOURCES OF NONLINEARITY

Track structures are complex multi-body, multi-interaction structures that undergo a variety of failure mechanisms. Referring to Fig. 2 in Chapter II once again, it might be useful to remind the reader that the track structure is composed of two rails, connected to the crossties by pins, which are in turn staked into the ballast and rest on an elastic foundation. Each component of the structure interacts with each other: the crossties provide the structure with additional resistance to bending, while the ballast provides stability, drainage and resistance to motion due to the ballast-tie interface friction and finally, the elastic foundation provides resistance to out of plane motion. These interactions necessarily make the problem quite complex to model, and furthermore, the degree of complexity increases significantly due to the nonlinear nature of the processes involved. Therefore, it is imperative to identify and understand how these nonlinearities affect rail buckling. Briefly, the present research focuses on the following distinct modes of nonlinearity, which will be discussed in detail below:

1. Geometric nonlinearity due to large deformations (buckling)
2. Nonlinearity in the friction field due to track lift-off
3. Constitutive nonlinearity due to nonlinear friction at the ballast tie interface
4. Geometric nonlinearity due to track misalignment

First of all, rail buckling is the formation of a sudden large, lateral misalignment of the tie-rail system. Fig. 15, below, shows a depiction of asymmetric (S-shaped) buckling of the tie-rail system. Note that, rails can also buckle symmetrically (U-shaped), and one such example can be observed in Fig. 1, located in Chapter I of this dissertation.

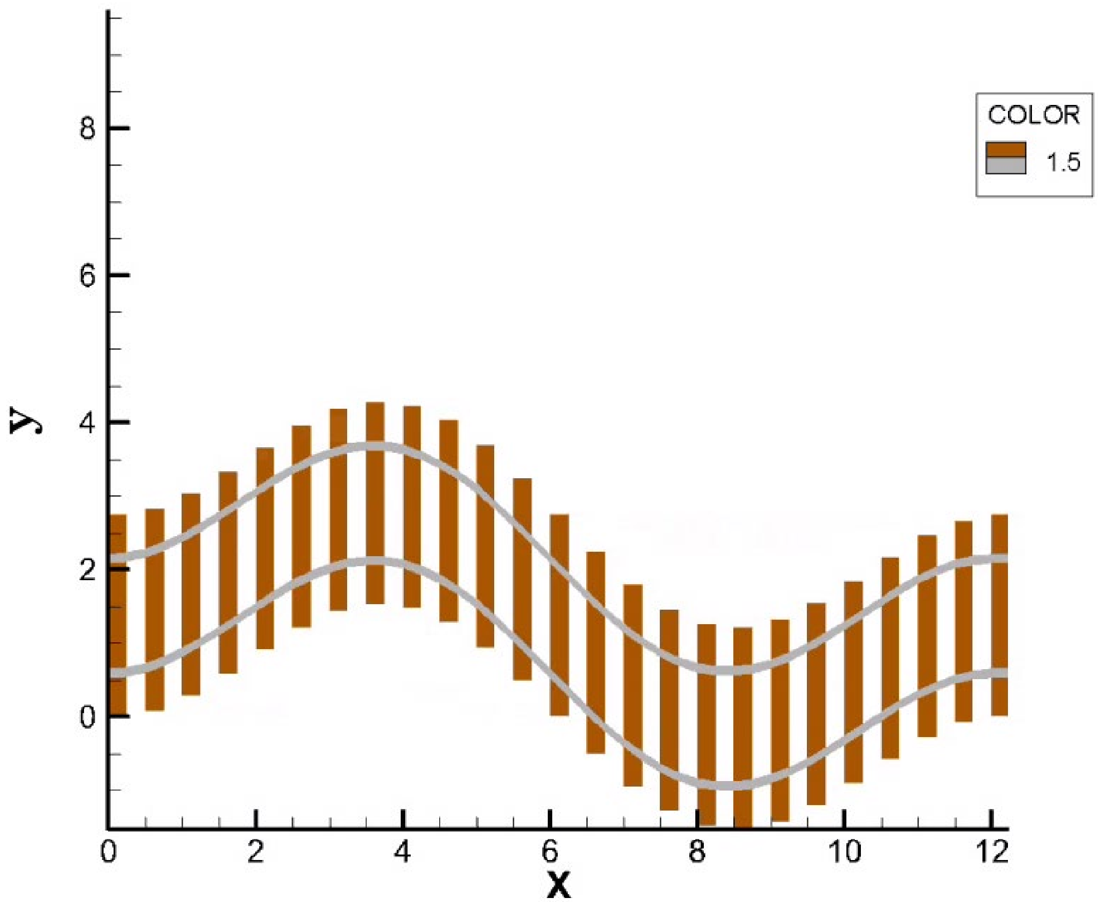

Figure 15. Depiction of Asymmetric, S-shaped, Buckling of the Tie-Rail System

Rail buckling is caused primarily by high compressive forces, usually a combination of mechanical and thermal compressive loading, vehicle loading and weakened track conditions. It is geometrically nonlinear due to large deformations, which essentially means that the axial loading affects the transverse displacements due to the fact that the deformed configuration of a differential element of the rail cannot be accurately approximated by its undeformed configuration. This nonlinearity can be observed mathematically by the inclusion of higher order terms in Equation 8, which can be found in Chapter II, thus defining the strains through the use of the Green-Lagrange strain tensor. Furthermore, the equations of equilibrium are necessarily formulated in the deformed configuration, which implies that changes in the geometry under loading are significant and have to be considered. Mathematically speaking, this implies that there exists a distinction between the spatial and material coordinate frame of reference: equation (35), below, illustrates how the spatial coordinates of a material point, x_i, differ from the material coordinates, X_i, by the displacement vector u_i (Lai et al. 2010), illustrated in Fig. 16.

$$x_i = X_i + u_i \tag{35}$$

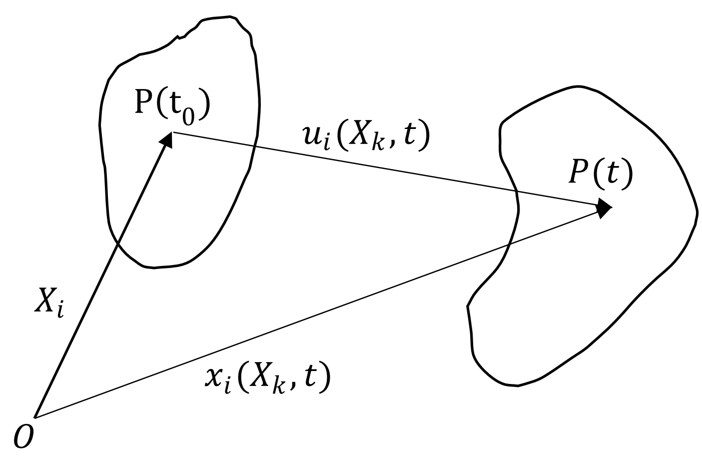

Figure 16. The displacement vector of a particle in a continuum (identified by its material coordinate X_i), from the reference position $P(t_0)$ to the current position $P(t)$,is given by the displacement vector u_i

These conditions necessarily cause the response of the rail undergoing buckling to be geometrically nonlinear.

Next, let's consider track uplift. Based on industry observations, lift-off of the rail-tie system will necessarily cause the rail to buckle laterally: train engineers have reported that, when vertical vehicle loads are large enough, the rail-tie system lifts from the ballast ahead of the train and immediately buckles laterally; in such cases, it is typical for the engineer driving the train to witness the buckle happen in real time, which often causes the entire train to derail. In general, lift-off induced buckling occurs due to the geometry of the rail structure and the loss on friction the ballast typically would exert on the track during downward vertical motion. Figure 17, shown below, depicts this phenomenon.

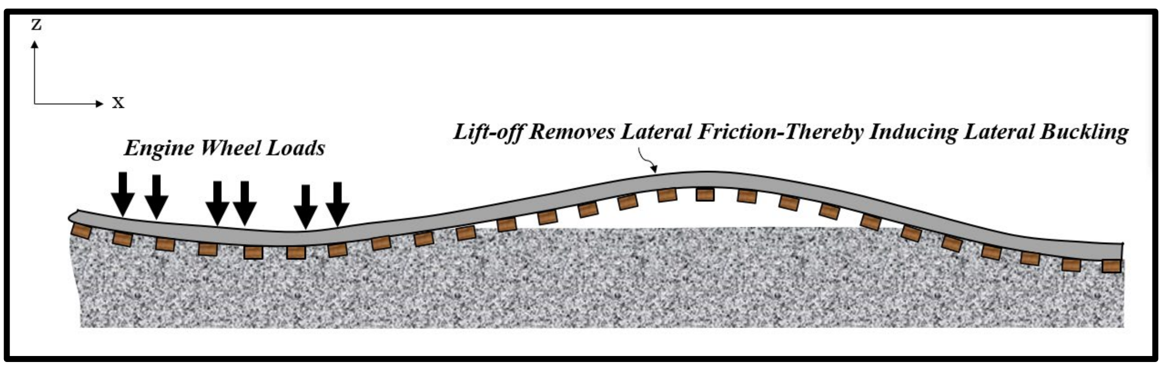

Figure 17. Depiction of the Rail Lift-Off Problem (Reprinted with Permission from Musu 2021)

Firstly, due to the geometric shape of the rail cross-section, buckling normally occurs in the horizontal x-y plane, meaning that the rail will fail about the weak z-z axis. This is due to the fact that, for rails of typical cross-section, Equation (36) controls failure due to bending such that buckling vertically, about the y-axis, rarely if ever happens in rails.

$$I_{yy} \gg I_{zz} \tag{36}$$

Thus, even when the rail bends about the y axis, buckling will occur laterally, about the z axis. Additionally, lift-off of the track structure from the ballast removes the resistance to buckling caused by the ballast-crosstie interface friction, thereby inducing buckling. This loss of friction introduces a significant source of nonlinearity into the problem.

$$\forall\, w(x) > 0 \quad \Rightarrow \quad k_x = k_y = k_z = 0 \tag{37}$$

Equation (37) represents a strong nonlinearity as it introduces a jump discontinuity in the friction field, which is a nonlinearity in the constitutive behavior of the friction field any time lift-off occurs.

Now, let's consider once again the friction the ballast exerts on the tie-rail system. A nonlinearity will necessarily be introduced whenever the coefficients of friction, k_x and k_y, are not constant, and this circumstance closely resembles the real-world physics of the rail structure. The nonlinearity enters via the dependence of the friction coefficients on the displacement components, *u* and *v,* respectively. As shown in Fig. 18, single tie push tests (STPT) confirm the nonlinearity for the lateral coefficient k_y.

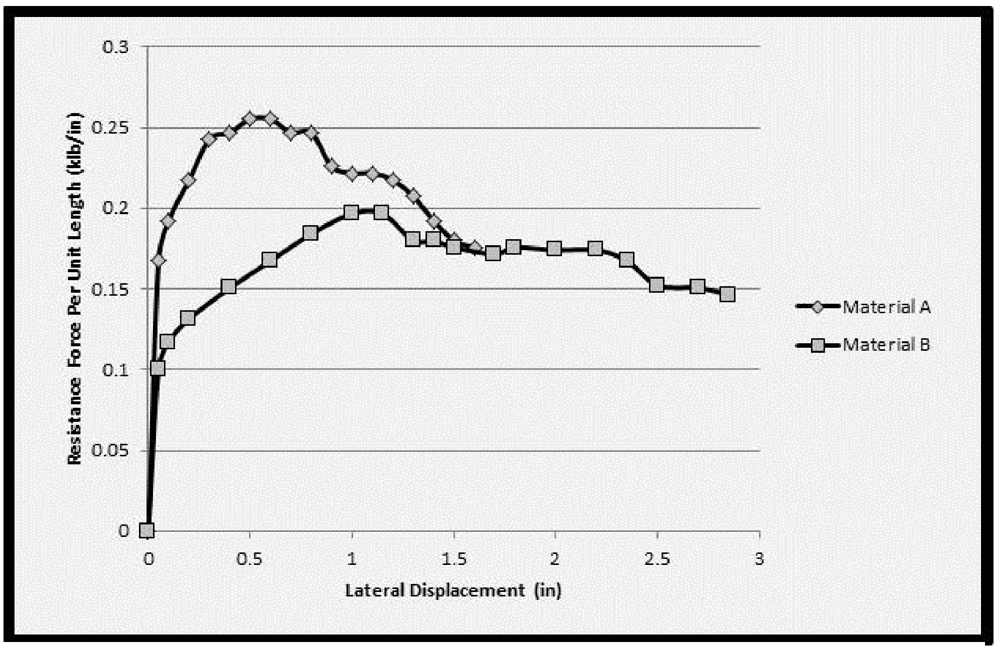

Figure 18. Typical Lateral Load vs. Displacement from STP Tests (Read et al. 2011)

For a given rail structure configuration, the above response may be adequately modeled with a power law of the following form (Tvergaard and Needleman 1981, Allen et al. 2016):

$$k_y(v) = k_y^0 - k_y^1 \left(\frac{v}{v_0}\right)^n \tag{38}$$

It should be noted that piecewise linear (Lim et al 2003), hyperbolic tangent equations (Grissom and Kerr 2006) and even upper limiting values (Grissom and Kerr 2006) have been used to curve fit the response illustrated in Fig. 18. However, the predicted buckling results do not appear to be very sensitive to the form of equations used. Thus, the power law form given by equation (38) is employed in this research. As shown in Fig. 19, this type of curve fit does an adequate job of predicting the observed nonlinearity in the coefficient of lateral friction. Accordingly, the same type of equation is employed for the longitudinal coefficient of friction. As can be seen from Fig. 18, the coefficient of lateral friction can be highly nonlinear. Accordingly, failing to account for this nonlinearity in the model can lead to significant predictive error.

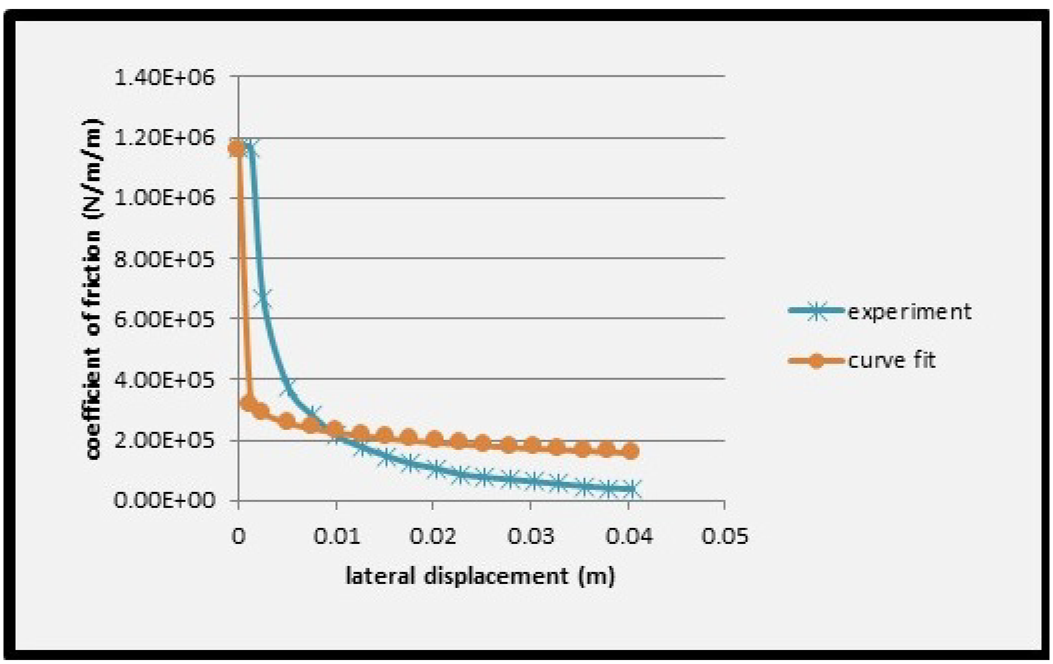

Figure 19. Comparison of Predicted Coefficient of Lateral Friction to Experimental Data Using Equation 38 (Reprinted with Permission from Allen and Fry, 2017)

Additionally, let's consider so-called "track-walk", which is the introduction of a lateral deviation in the layout of the rail usually caused by vehicle loads, base degradation or other weakened track conditions. This deviation is essentially an eccentricity that causes the rail to displace from its initially straight configuration thereby creating small lateral misalignment of the rail. This so-called track-walk is observed to reach magnitudes as large as five centimeters, and it is therefore an important source of nonlinearity in the problem. It is considered a geometric nonlinearity inasmuch as the eccentricity induces additional secondary moments, thereby significantly reducing the buckling load. Within this thesis it is assumed that the buckling load is reduced by the amount of loading necessary to produce a given amount of track-walk (Fig. 20), and this relationship is shown to be quasilinear.

Figure 20. Axial Load Required to Induce a Certain Amount of Initial Lateral Misalignment of the Rail-Crosstie System

Rail structures are also known to experience a variety of other nonlinear processes. Among these, some of the most important are buckling due to the presence of moisture on the track and buckling on curves. While these two nonlinearities are not strictly the focus of this work, the author believes it is important to briefly explore their effects on the rail structure in order to paint the full picture of the complexity of the rail buckling problem and the mechanisms involved.

Ballast degradation is reported to be one of the most common causes of inadequate track performance. In general, it usually refers to the mechanisms that jeopardize the ability of the ballast to provide structural stability for the track, drainage and resistance to motion due to the friction exerted by the ballast on the rail-tie system. One such mechanism is fouling, which is essentially a contamination of the ballast that occurs when the voids in between the ballast grains are either entirely or partially filled by fine particles. This fouling can be caused by a variety of factors, including wind, cyclical vehicle loading and the migration of fines from either the subgrade or the surroundings. One of the major consequences of ballast fouling is the reduced ability or complete failure of the ballast to provide adequate drainage after a rainfall event. Furthermore, the presence of moisture on the track can cause a reduction in the friction force exerted by the ballast on the tie-rail system, which will also dramatically decrease the track buckling load. It is a strong nonlinearity due to the fact that it causes a jump discontinuity in the friction field, much like in the lift-off problem.

Based on industry observations, curved sections of the rail structure have also been reported to undergo buckling. It is understood that buckling on curves occurs due to the influence of residual stresses and geometric imperfections on the failure mechanisms within the rail structure. Much like the misalignment problem, these geometric imperfections cause the induction of additional secondary moments that then reduce the buckling load, a phenomenon that is considered a geometric nonlinearity. Additionally, the problem of buckling on curves is made even more complex by the introduction of the residual stresses necessary to bend the track as required and that are largely unknown, as well as by additional complexity associated with the more complex numerical models that must be implemented to account for the track curvature.

Finally, it is important understand that while all these nonlinearities have so far been treated separately by the authors, the real-world physics of the rail shows that all of these mechanisms can and do occur simultaneously, and it is therefore necessary to develop a model that is capable of handling some or all of these distinct modes of nonlinearity concurrently. With the exception of curved track, this has been accomplished within this dissertation.

CHAPTER VI

RESULTS

The following sections of this report illustrate the results of the research efforts to date. Briefly, these efforts are focused on mitigating rail buckling via sensitivity analysis. Most recently, the focus has been on modeling the effects of rail lift-off on lateral buckling.

ANALYSIS OF SENSITIVITY OF BUCKLING DUE TO VARIATIONS IN RAIL PHYSICS

The rail buckling model developed herein is being deployed for the purpose of prioritizing rail buckling mitigation strategies. Toward this end, buckling sensitivity studies have been performed as functions of the following input variables: temperature change (ΔT), lateral friction coefficient (k_y) and the track modulus (k_z).

We define herein the sensitivity as the rate of change of the buckling load with respect to the input variable of interest. It can be seen that this is represented by the slope in the following diagrams, whereby the effects on the buckling load due to a change in the variable of interest can be assessed. Symmetric (u-shaped) buckles were modelled on 20-meter-long sections of the rail, induced by monotonically increasing the loading until buckling occurs in the rail structure. Note that the AREMA 115L-10 rail head section was chosen to represent a generic rail of typical dimensions, in accordance with industry specifications (Nippon Steel Corporation 2020) such that the response of a realistic rail section could be modeled.

Temperature Sensitivity

First consider the sensitivity of the buckling load to temperature change. As shown in Fig. 21, the predicted buckling load decreases with increasing temperature change. It can be observed that there is a noticeable decrease in sensitivity of the buckling load to temperature change with increasing temperature change.

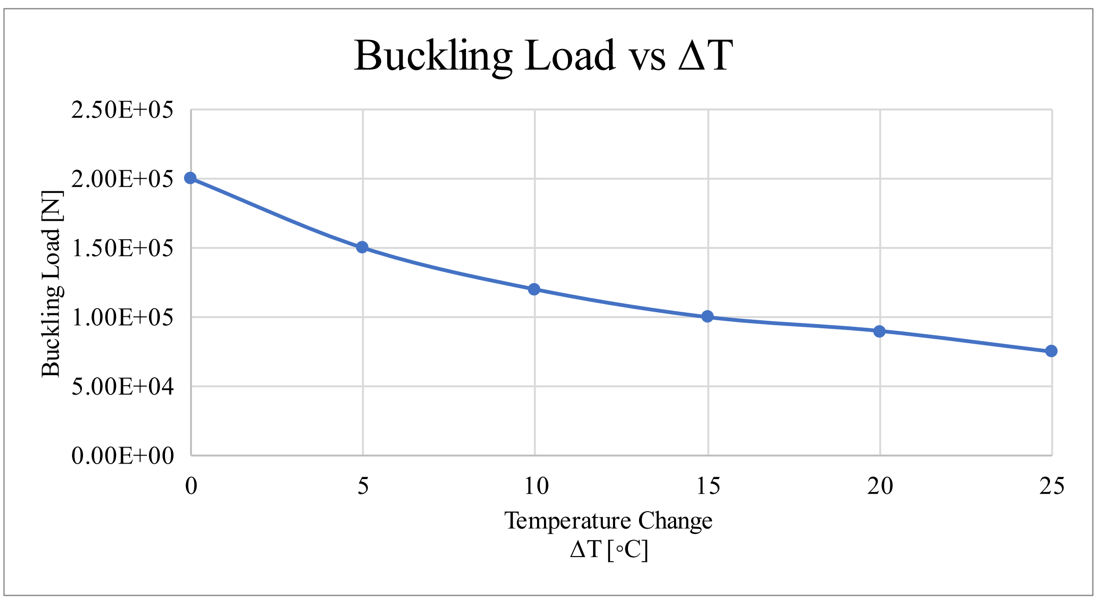

Figure 21. Predicted Effect of Temperature Change on Buckling Resistance of a Typical Rail Structure

Constant Lateral Coefficient of Friction Sensitivity

Consider now the sensitivity of the buckling load to changes in the constant lateral coefficient of friction, k_y, which represents the transverse component of friction between the ballast and the crosstie. As shown in Fig. 22, the predicted buckling load increases with increasing coefficient of lateral friction. Furthermore, a slight increase in the sensitivity of the buckling load can be observed with increasing ballast-crosstie friction.

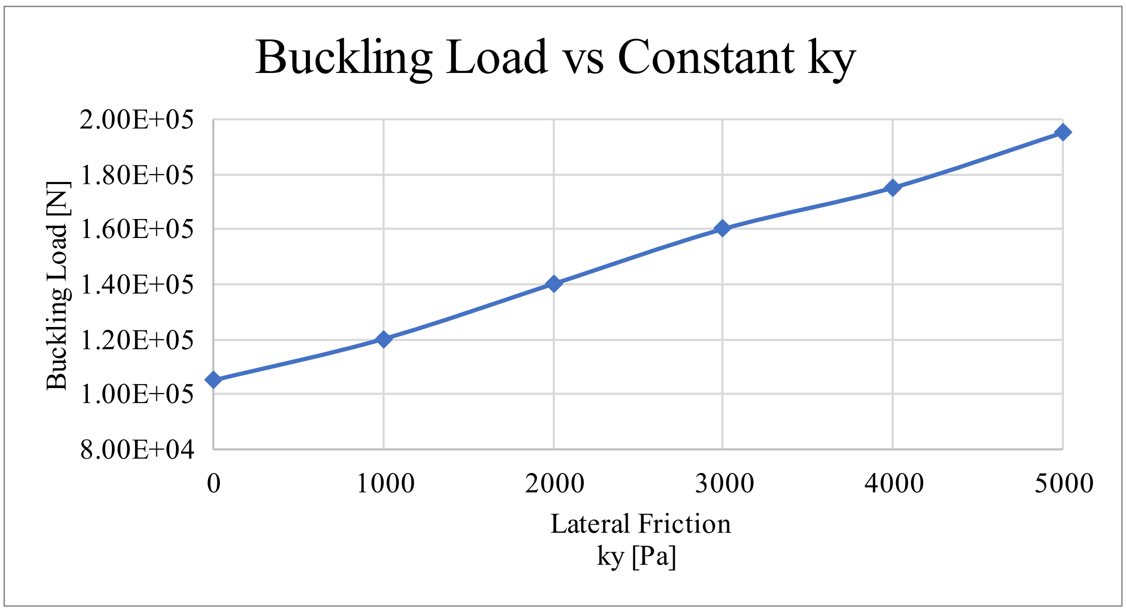

Figure 22. Predicted Effect of Constant Ballast-Crosstie Coefficient of Lateral Friction Change on Buckling Resistance of a Typical Rail Structure

Track Modulus Sensitivity

Finally, consider the sensitivity of the buckling load to changes in track modulus, k_z, which acts at the interface of the ballast with the rail structure. The track modulus is therefore defined as a measure of the vertical stiffness of the rail foundation (Selig and Li 1994), which represents the elastic modulus of the foundation. In order to fully investigate the sensitivity of the buckling load to changes in track modulus, it was necessary to consider how a stiffer foundation affects the response of the rail structure: for foundations with increasing stiffness it is expected that the rail will lift-off from the foundation ahead of the train, thus removing the resistance to buckling caused by the ballast-crosstie interface friction. Thus, the sensitivity to changes in the magnitude of the track modulus is shown in Fig. 23. It can be clearly inferred that the buckling load is significantly affected by changes in track modulus when the track structure experiences lift-off for relatively low values of the track modulus. The sensitivity for this case is highly nonlinear, and it can be seen that the data agrees with the expected response of the rail structure such that lift-off resulting from a softer foundation removes resistance due to lateral friction, thereby dramatically reducing the buckling load.

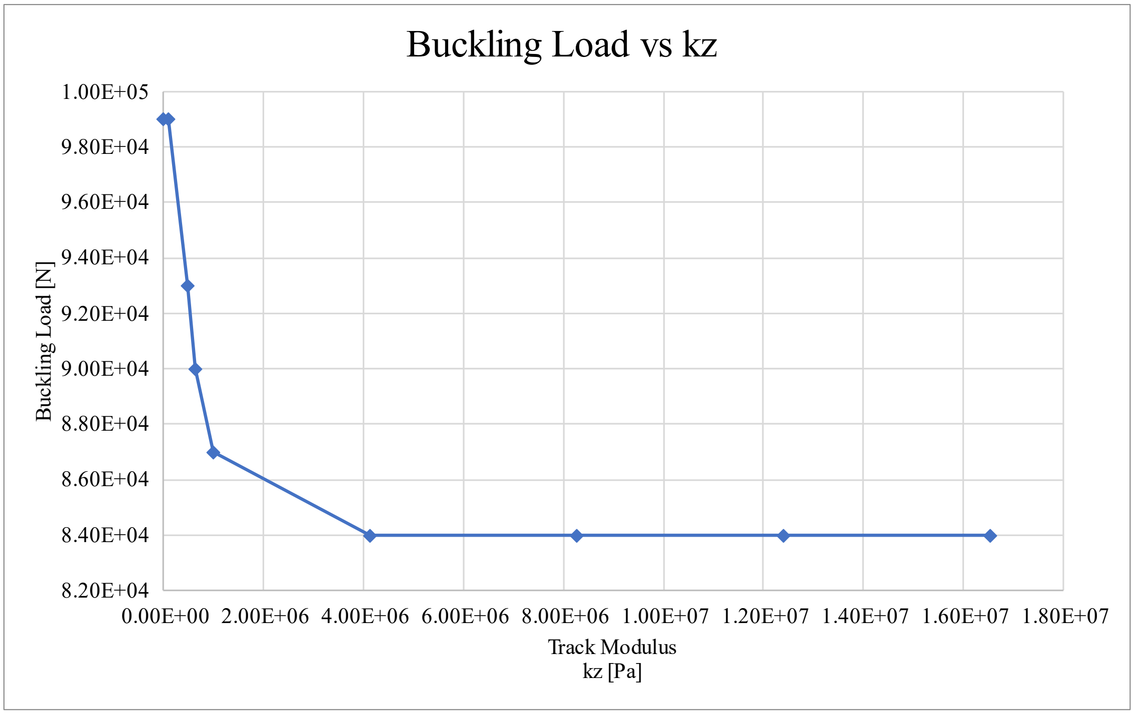

Figure 23. Predicted Effect of Track Modulus on Buckling Resistance of a Typical Rail Structure for the Case of Lift-Off of the Structure

SUMMARY OF LIFT-OFF INDUCED LATERAL BUCKLING

The model presented herein was deployed in an effort to demonstrate the effects of track lift-off on lateral buckling, with the objective of validating the following hypotheses:

1. Lift-off is inversely proportional to the track modulus (k_z)
2. The buckling load is a strong function of the track modulus (k_z) when lift-off occurs
3. When lift-off does not occur the buckling load is a weaker function of the track modulus (k_z)

Due to the geometric shape of the cross-section of the rail, buckling vertically (about the y axis) rarely if ever happens in rails. Based on industry observations, what typically happens is that the rail lifts vertically and buckles laterally.

In order to accurately predict the response of the rail structure to vertical displacement, the same assumption has been deployed in at least one more complex model (Dong, Sankar and Dukkipati 1994) as shown in equation (37) and reported in Chapter V. Equation (37) ensures that whenever the track system lifts-off from the ballast the coefficients of friction are taken as zero. This relationship is checked at every time step and iteration within the algorithm. It can be shown that the buckling load decreases significantly with lift-off of the track structure and is thus dependent on the track modulus. Furthermore, it can be shown that the track modulus significantly affects the length of the section of the rail that experiences lift-off, in turn also affecting the buckling load. In Fig. 24, the buckling load is shown as a function of the length of the lift-off for the same range of values of the track modulus studied in the previous sensitivity analysis. It can be seen that a stiffer foundation causes the rail to lift-off and the magnitude of the length of the lift-off increases with increasing track modulus, which in turn results in a dramatic decrease in the buckling load. Thus, it can be inferred that the buckling load is also a strong function of the lift-off length.

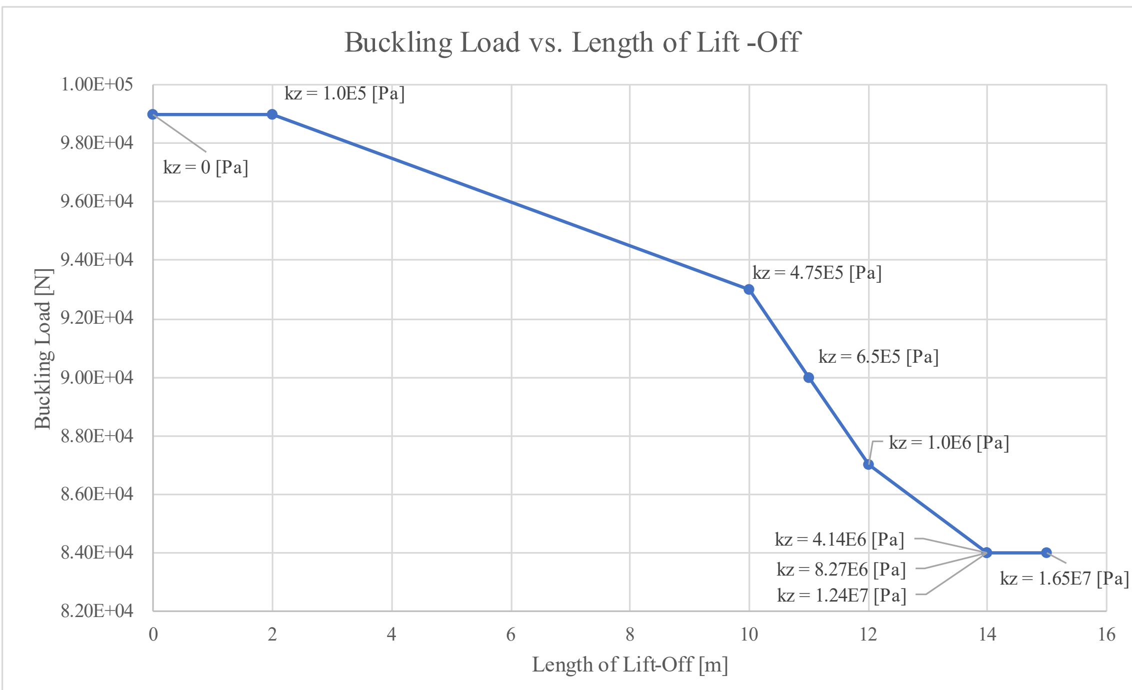

Figure 24. Buckling Load as a Function of the Length of the Lift-off for Varying Track Moduli

Note that the lift-off problem was modeled utilizing representative values of the coefficients of friction, as further research outside the scope of this dissertation is expected to properly establish realistic friction coefficients for the rail structure. However, the track modulus was estimated to typically range between 4.14E6 – 1.65E7 Pa (Kerr 2000) for rail structures, and this range has been included in the analysis.

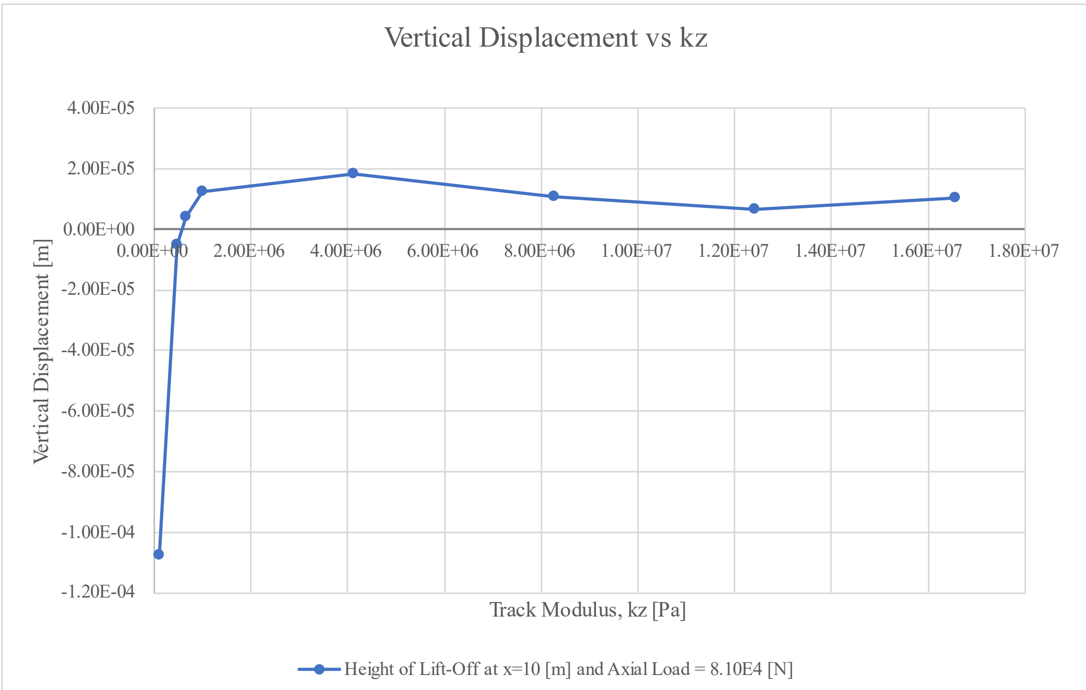

Figure 25. Vertical Displacement as a Function of the Track Modulus

Finally, Fig. 25 shows the vertical rail displacement as a function of the track modulus taken at the location of maximum transverse displacement, and at a constant load. It can be seen that as the rail lifts-off, the vertical deformation is weakly dependent on the track modulus. However, it is significant to note that the buckling load is virtually insensitive to changes in the magnitude of the vertical displacement at lift-off. Thus, rail buckling is predicted to occur at lift-off independently of the magnitude of the vertical displacement of the rail.

SUMMARY OF THE TRACK MISALIGNMENT BUCKLING PROBLEM

The model presented herein has been deployed in an effort to demonstrate the effects of track misalignment on lateral buckling, with the objective of validating the hypothesis that track-walk, caused by cyclical vehicle loading, induces an eccentricity in the geometric configuration of the rail, which in turn induces additional secondary moments, thereby dramatically reducing the buckling load. Fig. 26 shows the predicted effects of increasing lateral track-walk on the buckling load for a typical rail-structure subjected to mechanical and thermal loading. In this case, the thermal loading is due to the temperature change experienced by the rail from the rail neutral temperature (RNT). Rail neutral temperature is defined as the stress-free state of the rail, it is essentially the temperature at which the rail experiences zero internal forces.

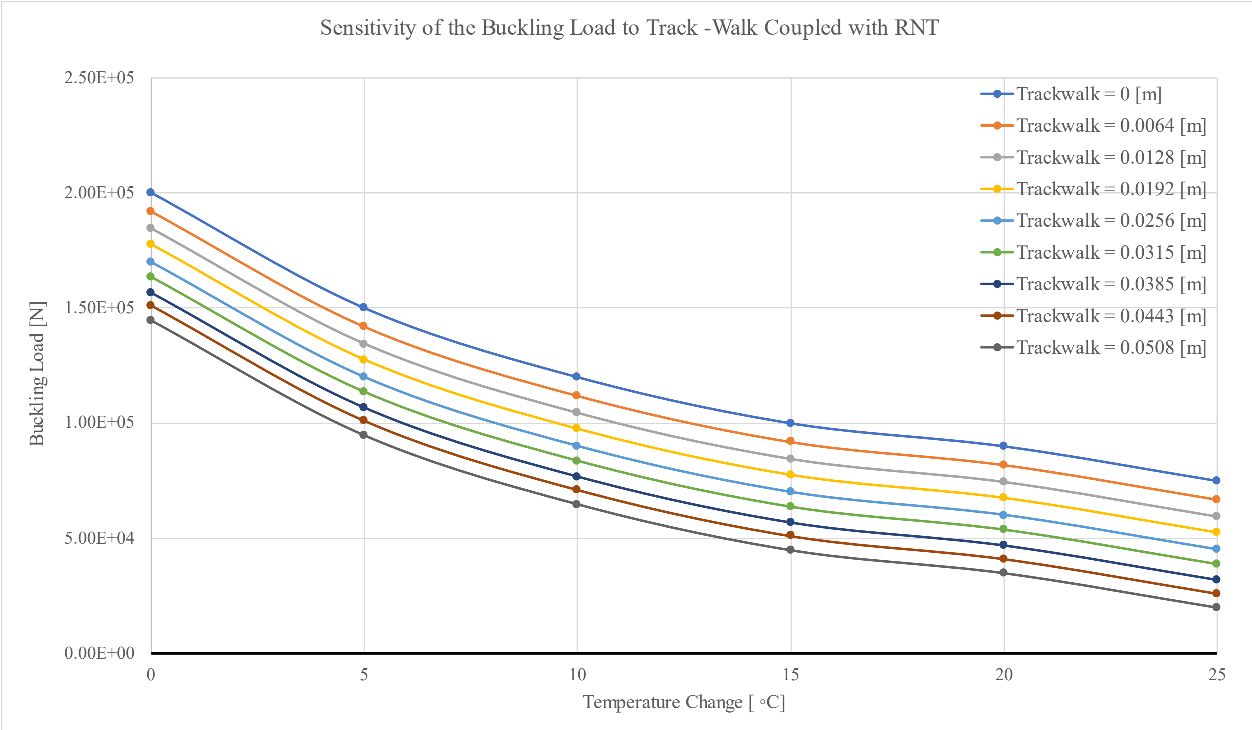

Figure 26. Predicted Effects of Track-Walk on Buckling Resistance of a Typical Rail Structure for the Case of Coupling with RNT

Fig. 26 thus, shows that for varying deviations from the rail neutral temperature, track misalignment dramatically reduces the buckling load. Specifically, the buckling load is observed to decrease for increasing temperature change, with a noticeable decrease in sensitivity with increasing temperature change. Furthermore, it can be observed that increasing track misalignment further decreases the buckling load quasi-linearly. Changes in the magnitude of the misalignment of at least 2.5 centimeters are observed to affect the buckling load significantly, reducing it by about 15-40% for the range of RNT considered.

Consider now the sensitivity of the buckling load to changes in the nonlinear lateral coefficient of friction, k_y, which represents the transverse component of friction between the ballast and the crosstie. The nonlinearity is modelled as described in Chapter V, and it was included in order to better represents the real-world physics of the rail.

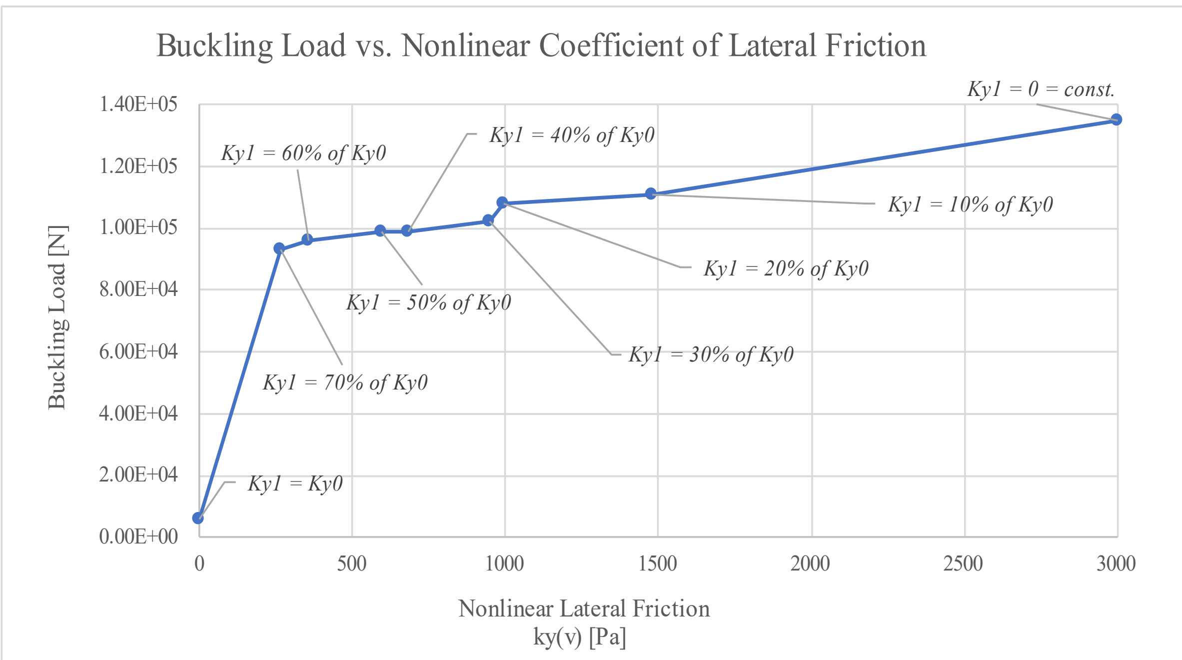

Figure 27. Predicted Effects of Nonlinear Lateral Friction on Buckling Resistance of a Typical Rail Structure

As shown in Fig. 27, the predicted buckling load increases with increasing coefficient of friction, in agreement with the constant friction case. However, this case is highly nonlinear, and an increase in the sensitivity of the buckling load can be observed with increasing lateral friction. Furthermore, Fig. 28 shows the coefficient of lateral friction varies as a function of the lateral displacement for the cases where k_y^1 was reduced between 10% and 70% of k_y^0, and including the limiting cases where $k_y^1 = 0$ and $k_y^1 = k_y^0$. Note that Fig. 28 shows how the coefficient of lateral friction varies with respect to the lateral displacement of the rail at the point of maximum displacement until buckling occurs. Note that the behavior agrees with the curve-fit obtained using equation (38) and shown in Fig. 19 in Chapter V.

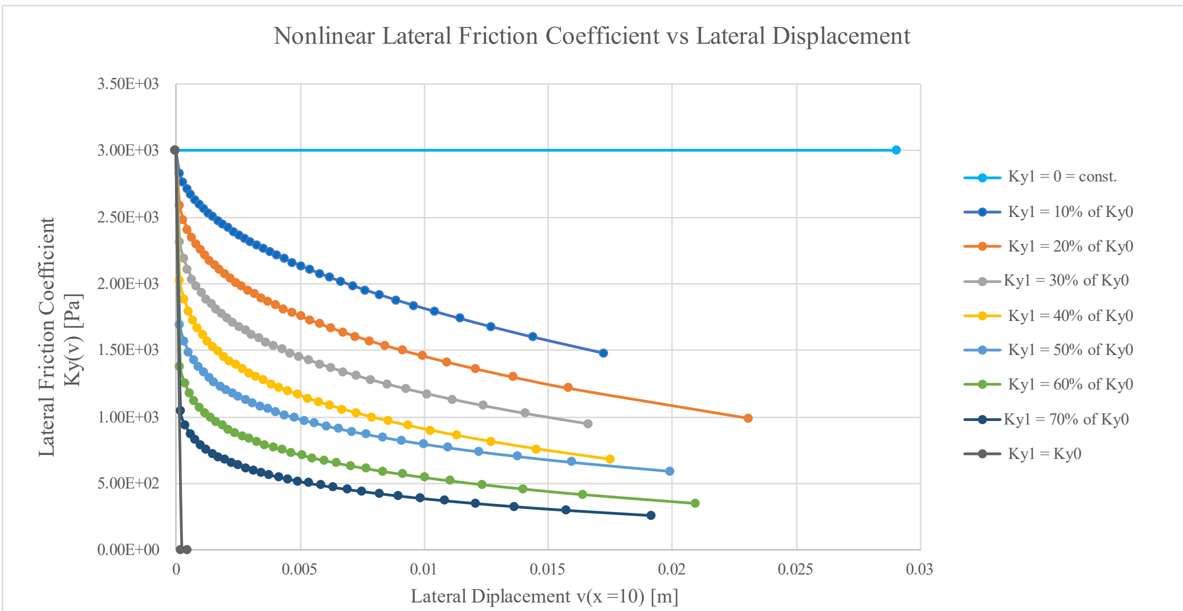

Figure 28. Nonlinear Coefficient of Friction as a Function of the Lateral Displacement at the Point of Maximum Displacement for Varying Values of k_y^1, Including Limiting Cases, for a Typical Rail Structure

CHAPTER VII

CONCLUSIONS

A formulation has been presented herein for the purpose of modeling lateral buckling in rail structures resting on ballast with both longitudinal and lateral nonlinear friction coefficients, misalignment and possible lift-off, thereby producing multiple distinct modes of nonlinearity, and this formulation has been cast within a nonlinear finite element formulation. The formulation has been validated against both linear and nonlinear example problems where closed-form solutions exist, and it has been shown that the formulation presented herein is accurate and efficient when compared to existing analytical solutions.

Unfortunately, due to the multiplicity of nonlinearities present in track structures, analytical solutions do not exist for the vast majority of realistic circumstances, and this comprises the primary necessity for producing the computational model developed herein.

It is important to note that, while previous models with a similar theoretical background exist, analytical solutions were obtained by greatly simplifying the problem, therefore reducing the ability of the model to represent the real-world physics of the rail. Thus, because of the computational nature of the model presented herein, it quite possibly represents the single most general specialized, open source, computational algorithm ever written for rail buckling, as it is capable to handle simultaneously nonlinear buckling, rail lift-off, nonlinear friction at the ballast-tie interface, rail misalignment, the effects of rainfall on the track, lateral and vertical vehicle loads as well as additional rotational stiffness due to the presence of the ties. Moreover, it is significant to note that, while it is possible to model rail structures utilizing commercially available finite elements codes, doing so greatly increases the degree of complexity associated with modeling the rail buckling problem, while also reducing efficiency, providing little to no additional accuracy, as well as being quite costly. Therefore, it is envisioned that the relatively simple but powerful nature of the model presented herein has the capability to greatly impact the rail industry by providing railway engineers the means to assess the necessity for intervention and/or replacement of sections of the track structure for the purpose of avoiding costly and sometimes life-threatening track buckles. Toward this end, the present model has been deployed in order to demonstrate its application to realistic rail structures. It is therefore envisioned that this algorithm can be a useful tool for developing rail buckling mitigation strategies.

Finally, while present research has focused on demonstrating the ability of the model to handle disparate but distinct modes of nonlinearity, further research will focus on modeling the effects of moisture on the track and buckling on curved track, as well as the interaction of all the distinct modes of nonlinearities presented herein that are observed to occur simultaneously in rail structures. It is also important to note that, while the author believes the code to be accurate in representing the physics of the problem at hand, other sources of uncertainties may exist and should be considered when attempting to predict buckling in rails. In general, the accuracy of the prediction is limited by the ability of current technology to accurately measure:

1. The rail neutral temperature (RNT)

2. The ballast-crosstie friction
3. The effects of moisture absorption, mud pumping and track tonnage on the ballast-crosstie friction
4. The track modulus along the track
5. The rotational stiffness due to the crossties
6. The effects of broken spikes and pins and the rail's resistance to bending

Therefore, further research should necessarily also focus on developing a methodology to approximate and reduce such uncertainties, in order to further improve the industry's ability to predict and prevent costly and sometimes life threatening rail buckles.

REFERENCES

D Allen and W Haisler (1985) Introduction to aerospace structural analysis, Wiley

D Allen (2013) Introduction to the mechanics of deformable solids: bars and beams, Springer

D Allen, G Fry and D Davis (2016) Development of a Model for Describing Nonlinear Lateral Resistance of Track Ballast, Technology Digest, TD-16-029

D Allen, G Fry (2017) Finite Element Formulation and Verification for Thermal Buckling of Rail Structures in the Horizontal Plane, CRR Report No. 2017-01

M A Crisfield (1981) A fast incremental/iterative solution procedure that handles "snap-through". In Computational methods in nonlinear structural and solid mechanics (pp. 55-62). Pergamon.

R.G Dong, S Sankar and R.V Dukkipati (1994) A Finite Element Model of Railway Track and its Application to the Wheel Flat Problem. Proceedings of the Institution of Mechanical Engineers, Part F: Journal of Rail and Rapid Transit, 208(1), 61–72.

L Euler (1744) Method inveniendi lineas curvas, Opera Omni, St. Petersburg, Russia

G Galileo (1637) Dialogues concerning two new sciences, Dover

G Grissom and A Kerr (2006) Analysis of lateral track buckling using new frame-type equations, Int J Mech Sci, 48:21-32

R E Hobbs (1984) In-Service Buckling of Heated Pipelines. Journal of Transportation Engineering, vol. 110, no. 2, 1984, pp. 175–189., https://doi.org/10.1061/(asce)0733-947x(1984)110:2(175).

S Kaewunruen, T Lewandrowski and K Chamniprasart (2018) Dynamic Responses of Interspersed Railway Tracks to Moving Train Loads. International Journal of Structural Stability and Dynamics, 18, 1850011.

A Kerr (1974) The stress and stability analyses of railroad tracks, J Appl Mech, 41:841-848

A Kerr (1978) Analysis of thermal track buckling in the lateral plane, Acta Mechanica, 30:17-50

A Kerr (2000) On the determination of the rail support modulus k, International Journal of Solids and Structures 37(32):4335-4351

A Kish, and G Samavedam (1982) Analysis of Thermal Buckling Tests on United States Railroads, DOT/FRA/ORD-82/45

A Kish, G Samavedam and D Jeong (1985) Influence of Vehicle Induced Loads on the Lateral Stability of CWR Track, DOT/FRA/ORD-85/03

A Kish and G Samavedam (1997) Longitudinal Force Measurement in Continuous Welded Rail from Beam Column Deflection Response, AREA Bulletin 712, Vol. 88

A Kish and G Samavedam (1990) Analyses of Phase III Dynamic Buckling Tests, DOT/FRA/ORD-89/08

A Kish and G. Samavedam (1991) Dynamic Buckling Test Analyses of a High Degree CWR Track, DOT/FRA/ORD-90/13

A Kish and G Samavedam (1991) Dynamic Buckling of Continuous Welded Rail Track: Theory, Tests, and Safety Concepts, Transportation Research Record, 1289, Proceedings of Conference on Lateral Track Stability

A Kish, S Kalay, A Hazell, J Schoengart, and G Samavedam, (1993) Rail Longitudinal Force Measurement Evaluation Studies Using the Track Loading Vehicle, Bulletin 742, American Railway Engineering Association

A Kish, D.W Clark and W Thompson (1995) Recent Investigations on the Lateral Stability of Wood and Concrete Tie Tracks, AREA Bulletin 752, pp 248-265

A Kish and G Samavedam (1999) Risk Analysis Based CWR Track Buckling Safety Evaluations, Proceedings of Conference on Innovations in the Design and Assessment of Rail Track, Delft University of Technology, The Netherlands

A Kish, G Samavedam, and D Wormley (2001) New Track Shift Limits for High-Speed Rail Applications, World Congress for Railway Research (WCRR 2001), Cologne, Germany.

A Kish, T Sussman, and M Trosino (2003) Effects of Maintenance Operations on Track Buckling Potential, International Heavy Haul Association Technical Conference, Dallas, Texas.

A Kish and G Samavedam (2005) Improvements in CWR Destressing for Better Management of Rail Neutral Temperature, Transportation Research Board 2005 Annual Conference

A Kish and G Samavedam (2013). Track buckling prevention: theory, safety concepts, and applications (No. DOT/FRA/ORD-13/16). John A. Volpe National Transportation Systems Center (US).

J.W Klaren and J.C Loach (1965) Lateral Stability of Rails, Especially of Long Welded Rails, Question D14, ORE, Utrecht

S Kristoff (2001) Track Lateral Strength Measurements at Union Pacific Railroad Sites, Foster-Miller Report prepared for Union Pacific Railroad

M W Lai, et al. *Introduction to Continuum Mechanics*. Fourth ed., Elsevier, 2010.

S.R Li and R.C Batra (2007) Thermal buckling and postbuckling of Euler-Bernoulli beams supported on nonlinear elastic foundations. AIAA journal, *45*(3), 712-720.

N Lim, N Park and Y Kang (2003) Stability of continuous welded track, Computers & Structures, 81:2219-2236

D Little, D Allen and A Bhasin (2016) Modeling and Design of Flexible Pavements and Materials, Springer

D J Miles and C R Calladine (1999) Lateral Thermal Buckling of Pipelines on the Sea Bed. Journal of Applied Mechanics, vol. 66, no. 4, 1999, pp. 891–897., https://doi.org/10.1115/1.2791794.

A Miri et al. (2021) Analysis of Buckling Failure in Continuously Welded Railway Tracks, Engineering Failure Analysis, vol. 119, p. 104989, DOI: 10.1016/j.engfailanal.2020.104989.

V Musu (2021). Computational Model for Predicting Buckling in Rail Structures, An Unpublished Master's Thesis, Texas A&M University

Nippon Steel Corporation (2020) Rails, downloaded at: https://www.nipponsteel.com/product/catalog_download/pdf/K003en.pdf

J. Oden and E Ripperger (1981) Mechanics of elastic structures, Second Edition, McGraw-Hill

J Oden. *Finite Elements of Nonlinear Continua*. McGraw-Hill, 1971.

G.P Pucillo (2016) Thermal buckling and post-buckling behavior of continuous welded rail track, Vehicle System Dynamics, 54:12, 1785-1807, DOI: 10.1080/00423114.2016.1237665

Railroad Accident Statistics (2020) Federal Railroad Administration, downloaded at:http://safetydata.fra.dot.gov/officeofsafety/publicsite/Query/TrainAccidentsFYCYWithRates.aspx

D Read, R Thompson, D Clark and E Gehringer (2011) Results of Union Pacific concrete tie track panel shift tests, Technology Digest, TD-11-004

J Reddy (1984) An Introduction to the Finite element Method, McGraw-Hill

J Reddy (2005) An Introduction to the Finite element Method, Third Edition, McGraw-Hill

E Riks (1979). An incremental approach to the solution of snapping and buckling problems. International journal of solids and structures, 15(7), pp.529-551.

G Samavedam (1979) Buckling and Post Buckling Analyses of CWR in the Lateral Plane, British Railways Board, R&D Division, Technical Note, TN TS 34

G Samavedam, A Kish and D Jeong (1986) Experimental Investigation of Dynamic Buckling of CWR Tracks, DOT/FRA/ORD-86/07

G Samavedam, A Kish and D Jeong (1987) The Neutral Temperature Variation of Continuous Welded Rails, AREA Bulletin 712

G Samavedam, A Purple, A Kish and J Schoengart (1993) Parametric Analysis and Safety Concepts of CWR Track Buckling, Final Report, DOT/FRA/ORD-93/26

G Samavedam (1995) Theory of CWR Track Stability, ERRI Report, D202/RP3, Utrecht

G Samavedam, A Kanaan, J Pietrak, A Kish and A Sluz (1995) Wood Tie Track Resistance Characterization and Correlations Study, Final Report, DOT/FRA/ORD-94/07

G Samavedam (1997) Investigation on CWR Longitudinal Restraint Behavior in Winter Rail Break and Summer Destressing Operations, DOT/FRA/ORD-97/01

G Samavedam et. al. (1997) Analysis of Track Shift Under High-Speed Vehicle-Track Interaction, Technical Report DOT/FRA/ORD-97/02

G Samavedam and A Kish (2002) Track Lateral Shift Model Development and Test Validation, DOT/VNTSC/FRA Report

E Selig, D Li (1994) Track Modulus: Its Meaning and Factors Influencing It, Transportation Research Record, No. 1470, Railroad Research Issues, http://onlinepubs.trb.org/Onlinepubs/trr/1994/1470/1470-006.pdf

Taylor, Neil, and Aik Ben Gan (1986) Submarine Pipeline Buckling—Imperfection Studies. Thin-Walled Structures, vol. 4, no. 4, 1986, pp. 295–323., https://doi.org/10.1016/0263-8231(86)90035-2.

S Timoshenko (1915) Strength of rails, Transactions of the Institute of Ways and Communications, St. Petersburg, Russia

S Timoshenko (1927) Method of analysis of statical and dynamical stresses in rail, Proc. Second International Congress for thermal track buckling, Int J Mech Sci, 23:577-587 Applied Mechanics, Zurich

V Tvergaard and A Needleman (1981) On localized thermal track buckling, Int J Mech Sci, 23:577-587

G Yang and M.A Bradford (2016) Thermal-induced buckling and postbuckling analysis of continuous railway tracks. International Journal of Solids and Structures, *97*, 637-649.

Zhang, Weihan, and Stelios Kyriakides (2021) Controlled Pipeline Lateral Buckling by Reeling Induced Curvature Imperfections. Marine Structures, vol. 77, 2021, p. 102905., https://doi.org/10.1016/j.marstruc.2020.102905.